



# A novel coupling approach of smoothed finite element method with SPH for thermal fluid structure interaction problems

Ting Long<sup>a,b,c</sup>, Pengying Yang<sup>a,b,c</sup>, Moubin Liu<sup>a,b,c,\*</sup>

<sup>a</sup> BIC-ESAT, College of Engineering, Beijing 100871, China

<sup>b</sup> Institute of Ocean Research, Peking University, Beijing 100871, China

<sup>c</sup> State Key Laboratory for Turbulence and Complex systems, Peking University, Beijing 100871, China



## ARTICLE INFO

### Keywords:

Edge-based smoothed finite element method (ES-FEM)  
Smoothed particle hydrodynamics (SPH)  
Coupling algorithm  
Thermal-fluid-structure interaction (TFSI)

## ABSTRACT

Thermal-fluid-structure interaction (TFSI) problems are significant in science and engineering, and usually pose great challenges for numerical simulations due to the coupled effects of thermal convection, fluid flow and structure deformation. In this paper, a novel coupling approach of smoothed finite element method (ES-FEM) with an improved smoothed particle hydrodynamic (SPH) method is developed for TFSI problems. In the coupling approach, the edge based ES-FEM is used to model solid domain and the Lagrangian SPH is used to model fluid flow. In ES-FEM, the temperature and velocity gradient smoothing technique are applied over the edge-based smoothing domain for thermal structure coupling problems. In SPH, some state-of-art algorithms including kernel gradient correction (KGC) and particle shift technique (PST) are integrated to ensure computational accuracy for simulating thermal fluid flows. A ghost particle coupling algorithm is developed to handle fluid-structure interaction and fluid-structure conjugate heat transfer, and the kinematic condition, dynamics conditions and conservation of energy are satisfied. Four numerical examples are tested to demonstrate the effectiveness of the present coupling approach of ES-FEM-SPH for TFSI problems.

## 1. Introduction

Thermal-fluid-structure interaction (TFSI) problems widely exist in engineering and sciences, such as the cooling of electronic devices, energy harvesting devices in microsystems, additive manufacturing processes, food processing, float glass production, nuclear reactors, micro-electronic devices, coating and solar power [1–5]. TFSI problems involve coupled effects of coupled effects of thermal convection, fluid flow and structure deformation. Thermal stress and fluid pressure lead to solid deformation, while solid deformation leads to the change of flow field and then further changes the temperature field. The coupling among the three physical fields of fluid, solid and heat occurs simultaneously and bidirectionally. The TFSI problems are usually difficult for numerical simulations due to the inherent complex nonlinear feature and coupling effects of thermal convection, fluid flow and structure deformation.

A large number of numerical approaches have been applied to solve the TFSI problems. Generally, the Lagrangian mesh based methods, such as the Finite Element Method (FEM) [6], are applied to solve the solid domain and the Eulerian mesh-based method, such as the Finite Element Method (FEM) [7], the Finite Difference Method (FDM) [8] and

Finite Volume Method (FVM) [9], are applied to solve the fluid domain. There are two types of methods for coupling Lagrangian mesh and Eulerian mesh: one is based on the dynamic mesh technique, such as the Arbitrary Lagrangian Eulerian (ALE) method [10,11], the other is based on the fixed mesh technique, such as the Immersed Boundary Method (IBM) [12]. Al-Amiri and Khanafar [13] used the ALE method to study mixed convection in a lid-driven square cavity with hyper elastic bottom wall. They reported that the modulus of elasticity of the elastic bottom wall plays a significant role in increasing the heat transfer. Raisi and Arvin [14] utilized ALE method to investigate the TFSI problem in a fluid filled square cavity with an elastic structure. They studied the effect of Rayleigh number on the deformation of elastic structures. Ghalambaz et al. [15] used the ALE method to investigate the TFSI problem in a square cavity, which an oscillating flexible beam attached to a hot wall. The results show that increasing the amplitude the oscillating flexible beam can significantly increase the Nusselt number. Ismael and Jasim [16] also utilized ALE method to study the role of TFSI in the mixed convection in a square cavity, which the flexible beam is attached to the bottom wall of the cavity. The IBM method has also been used to study TFSI problems. Soti et al. [17] utilized the IBM method to simulating the problem of flow induced deformation of thin elastic structure coupled with convective heat transfer. Cai and Thorner [18] developed the discontinuous Galerkin method implemented in IBM for TFSI problems. Up to now the mesh based method occupies the dominant

\* Corresponding author.

E-mail address: [mbliu@pku.edu.cn](mailto:mbliu@pku.edu.cn) (M. Liu).

approach for TFSI problems. However, it is a great challenge for Eulerian mesh-based method to handle the problems with moving interface and free surface. These problems require special interface or free surface tracking methods such as Level set (LS) [19] and volume-of-fluid (VOF) [20]. The simulation of TFSI problem under pure Lagrangian scheme is very attractive because it can naturally handle the moving interface, free surface and without convection term.

In recent years, many particle approaches have been developed for simulating fluid flows with moving interface and free surface, such as moving particle semi-implicit (MPS) [21–23], smoothed particle hydrodynamics (SPH) [24], material point method (MPM) [25–27], particle finite element method (PFEM) [28] and so on. Recently, Gotoh and Khayyer et al. [29] reviewed some recent developments in the application of particle methods in coastal and marine engineering. Khayyer et al. also [30] developed fully-Lagrangian particle methods for fluid-structure interaction. Among these particle approaches, the SPH is one of most widely used particle method. The SPH method is a Lagrangian meshless approach to solve partial differential equations, and was originally invented in 1977 by Lucy [31] and Monaghan and Gingold [24,32]. It is then widely applied to fluid mechanics [33–39], impact dynamics [40–42], astrophysics, and other fields. Moreover, the SPH method has also been applied to flow convection problem [43–45], solid heat conduction problem [46–48], fluid structure interaction problem [49–51] and fluid-solid conjugate heat transfer problems [52]. Compared with the traditional mesh based method, the SPH method has unique advantages in the incompressible flow modeling with moving interface and free surface [53]. In this paper, the SPH approach is utilized for modeling thermal fluid flows.

In recent years, the fluid-structure interaction (FSI) problems have been studied by coupling the FEM with SPH [54–60], and the coupling approaches make full use of the advantages of SPH method in solving hydrodynamics and the advantages of FEM in simulating structural dynamics. Typical works include Vuyst [54], Groenboom and Cartwright, [55], Fourrey, [56,61], Yang [57], Hu et al. [58] and Long et al. [59]. In these works, FEM is utilized to model the movement and deformation of structures and SPH is utilized to model the fluid flows. To the best of the authors' knowledge, there are no available reports in open literature to develop coupling approach of FEM-SPH for modeling TFSI problems, mainly due to the inherent complex nonlinear feature and coupling effects of thermal convection, fluid flow and structure deformation in TFSI.

In addition, the conventional FEM is hindered with some drawbacks. It is known that the “overly-stiff” feature of the conventional FEM models usually leads to undesired results in practical numerical solutions by FEM and relevant coupling methods [62]. The smoothed finite element method (S-FEM) [63] proposed by Liu et al. provides an effective way to solve this problem in FEM, which is based on the gradient smoothing technique of the mesh-free method [64]. Many smoothing approaches have been developed, such as the cell-based [65], nodal-based [66], edge-based [67] and face-based [68] S-FEM. Furthermore, the edge based S-FEM (ES-FEM) has good performance even using the linear three-node triangular elements. In this article, the ES-FEM based on update Lagrangian description is developed for modeling coupled thermal elastic problems.

The objective of this paper is to develop a novel coupling approach of ES-FEM with SPH to simulate TFSI problems. In the present ES-FEM-SPH coupling approach, the Lagrangian ES-FEM is developed for modeling thermal structure coupling problems and the SPH is used for modeling thermal fluid flows. Ghost particle coupling algorithm developed by Long et al. [69] is utilized to treat fluid structure interaction and a ghost particle coupling algorithm is developed to handle fluid structure conjugate heat transfer.

The article is organized as follows. In Section 2, the ES-FEM based on updated Lagrangian formulation for thermal structure coupling problem is introduced. In Section 3, the SPH method with some accuracy and stability enhancing techniques for flow convection problem is concisely described. In Section 4, the ghost particle coupling schemes for fluid structure interaction and fluid structure conjugate heat transfer are described. Four numerical examples are provided in Section 5 to demonstrate the effectiveness of the present method for modeling TFSI problems. The paper ends in Section 6 with some concluding remarks.

## 2. ES-FEM formulations for thermal-structure coupling problems

In this section, the ES-FEM based on updated Lagrangian description for thermal structure coupling problems is developed and linear three-node triangular elements are utilized to discretize the domain. The smoothed shape function gradient, smoothed temperature gradient and the smoothed velocity gradient are then derived. The ES-FEM is then applied to discretize the governing equations of coupled thermal elastic problems and the corresponding ES-FEM formulations are obtained.

### 2.1. Governing equations

A homogeneous, isotropic and linear thermal elastic solid is considered. The governing equations for linear, dynamic, coupled thermal elastic problems in the time domain can be written as

$$\sigma_{ij,j} + b_i^s - \rho^s \ddot{u}_i^s = 0, \quad (1)$$

$$\rho^s c^s \dot{T}^s - k^s T_{,ii}^s + \beta^s T_0^s \dot{\epsilon}_v - Q = 0, \quad (2)$$

where  $\sigma_{ij}$  is Cauchy stress tensor,  $b_i^s$  is the body force,  $u_i^s$  is displacement vector component,  $\rho^s$  is the density of solid,  $c^s$  is the specific heat,  $k^s$  is the coefficient of thermal conductivity,  $T_0^s$  and  $T^s$  is the reference temperature and absolute temperature, respectively,  $\dot{\epsilon}_v$  is the bulk strain rate,  $Q$  is the rate of heat generation within the body per unit mass in unit time.

In addition,  $\beta^s$  is the stress temperature modulus, the expression is given as follows,

$$\beta^s = \alpha_T^s (3\lambda + 2\mu), \quad (3)$$

where  $\alpha_T^s$  is the coefficient of thermal expansion and  $\lambda, \mu$  are Lame constants.

For linear thermal elastic materials subjected to the temperature change, the thermal strain and stress are considered. The expression of thermal strain is given as

$$\epsilon_{ij}^0 = \alpha_T^s (T^s - T_0^s), \quad (4)$$

where  $\epsilon_{ij}^0$  is the thermal strain,  $v$  is the Poisson's ratio. Elastic strain equals total strain minus thermal strain, the expression of elastic strain is written as

$$\epsilon_{ij}^e = \epsilon_{ij} - \epsilon_{ij}^0, \quad (5)$$

where  $\epsilon_{ij}^e$  is the elastic strain,  $\epsilon_{ij}$  is total strain. The Saint-Venant-Kirchhoff constitutive model [70] is used in the this paper, the expression is given as

$$\sigma_{ij} = \lambda \epsilon_{kk}^e \delta_{ij} + 2\mu \epsilon_{ij}^e = \lambda \epsilon_{kk} \delta_{ij} + 2\mu \epsilon_{ij} - \beta^s (T^s - T_0^s) \delta_{ij}, \quad (6)$$

where  $\delta_{ij}$  is the Kronecker delta. In this paper, the stress update algorithm and Jaumann stress rates are used [70]. The relationship between Cauchy stress rate and Jaumann stress rate is given as

$$\dot{\sigma}_{ij} = \sigma_{ij}^\nabla + \sigma_{ik} \Omega_{jk} + \sigma_{jk} \Omega_{ik}, \quad (7)$$

where  $\sigma_{ij}^\nabla$  is the Jaumann stress rate,  $\Omega_{ij}$  is spin tensor. The Jaumann stress rate is obtained through the constitutive model, the expression is written as follows,

$$\sigma_{ij}^\nabla = C_{ijkl} (\epsilon_{kl} - \alpha_T^s T^s \delta_{kl}), \quad (8)$$

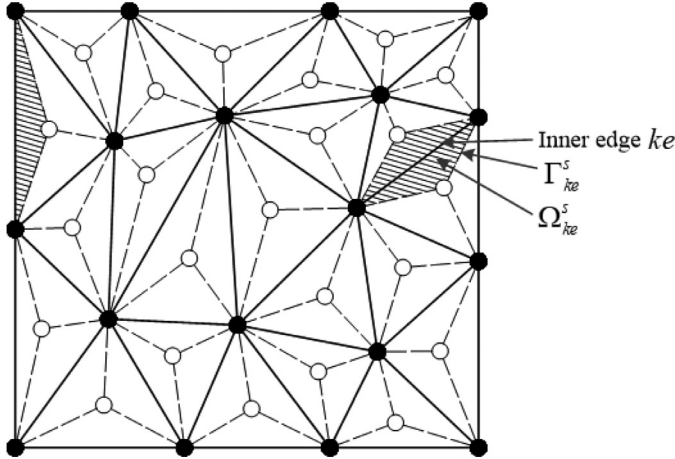


**Fig. 1.** ES-FEM-T3 settings: Triangular elements (solid lines) and the edge-based smoothing domains (shaded areas).

where  $C_{ijkl}$  is constitutive tensor. Using the Saint-Venant-Kirchhoff constitutive model, the Jaumann stress rate is obtained by

$$\sigma_{ij}^{\nabla} = \lambda \dot{\epsilon}_{kk} \delta_{ij} + 2\mu \dot{\epsilon}_{ij} - \beta^s \dot{T}^s \delta_{ij}. \quad (9)$$

## 2.2. ES-FEM with gradient smoothing technique

In ES-FEM, the velocity  $v_i^s$ , the current spatial position  $x_i^s$  and the absolute temperature  $T^s$  are approximated by

$$v_i^s = N_I v_{Ii}^s, \quad (10)$$

$$x_i^s = N_I x_{Ii}^s, \quad (11)$$

$$T^s = N_I T_I^s, \quad (12)$$

where  $N_I$  is the shape functions,  $x_{Ii}^s$  and  $v_{Ii}^s$  are the spatial position and nodal velocity component of the node  $I$ , respectively.  $T_I^s$  is the temperature of node  $I$ .

In ES-FEM, the calculation of the smoothed gradient of the field depends on a set of no overlap smoothing domains [71]. Herein, a smoothing domain setting of ES-FEM with triangle element is shown in Fig. 1. The smoothed velocity gradient of the smoothing domain  $\Omega_{ke}^s$  is defined as

$$\bar{v}_{i,j}^s = \frac{1}{A_{ke}^s} \int_{\Omega_{ke}^s} \frac{\partial v_i^s}{\partial x_j} d\Omega, \quad (13)$$

where  $A_{ke}^s$  is the area of the smoothing domain  $\Omega_{ke}^s$ . Applying a divergence theorem, the smoothed velocity gradient can be derived by

$$\bar{v}_{i,j}^s = \frac{1}{A_{ke}^s} \int_{\Gamma_{ke}^s} v_i^s n_j d\Gamma = \frac{1}{A_{ke}^s} \int_{\Gamma_{ke}^s} N_I v_{Ii}^s n_j d\Gamma = \overline{\left( \frac{\partial N_I}{\partial x_j} \right)} v_{Ii}^s, \quad (14)$$

where  $n_j$  is the unit outward normal vector of the smoothing domain boundary  $\Gamma_{ke}^s$ , and  $(\overline{\frac{\partial N_I}{\partial x_j}})$  is the smoothed derivatives of shape function defined as

$$\overline{\left( \frac{\partial N_I}{\partial x_j} \right)} = \frac{1}{A_{ke}^s} \int_{\Gamma_{ke}^s} N_I n_j d\Gamma. \quad (15)$$

Then, the smoothed temperature gradient  $\bar{T}_j^s$  can be derived by

$$\bar{T}_j^s = \overline{\left( \frac{\partial N_I}{\partial x_j} \right)} T_I^s. \quad (16)$$

Using the smoothed derivatives of shape function, it can easily construct the smoothed strain rate, the smoothed Jaumann stress rate, the smoothed Cauchy stress and so on.

## 2.3. ES-FEM formulations for coupled thermo-elasticity problems

### 2.3.1. Discretization for the momentum equation

Applying weak form Galerkin variational principle in ES-FEM, we can obtain

$$\int_{\Omega} \overline{\left( \frac{\partial v_i^s}{\partial x_j} \right)} \bar{\sigma}_{ji} d\Omega - \int_{\Omega} \delta v_i^s \rho^s b_i^s d\Omega - \int_{\Gamma_t} \delta v_i^s \bar{t}_i d\Gamma + \int_{\Omega} \delta v_i^s \rho^s \dot{u}_i^s d\Omega = 0, \quad (17)$$

where  $\delta v_i^s, \bar{t}_i, \bar{\sigma}_{ji}$  and  $\Gamma_t$  are the virtual velocity, the surface force, the smoothed Cauchy stress and the boundary of traction, respectively. Applying the shape function of linear polynomial interpolation, Eq. (17) can be written as

$$\int_{\Omega} \overline{\left( \frac{\partial N_I}{\partial x_j} \right)} \bar{\sigma}_{ji} d\Omega - \int_{\Omega} N_I \rho^s b_i^s d\Omega - \int_{\Gamma_t} N_I \bar{t}_i d\Gamma + \int_{\Omega} N_I \rho^s N_J \dot{u}_J^s d\Omega = 0 \quad \forall I \notin \Gamma_v, \quad (18)$$

where  $\Gamma_v$  is the boundary of velocity.

Finally, ES-FEM formulations for momentum equation are given as

$$M_I \ddot{u}_I^s + f_{Ii}^{\text{int}} = f_{Ii}^{\text{ext}}, \quad (19)$$

$$f_{Ii}^{\text{int}} = \int_{\Omega} \overline{\left( \frac{\partial N_I}{\partial x_j} \right)} \bar{\sigma}_{ji} d\Omega, \quad (20)$$

$$f_{Ii}^{\text{ext}} = \int_{\Omega} N_I \rho b_i d\Omega + \int_{\Gamma_t} N_I \bar{t}_i d\Gamma, \quad (21)$$

where  $M_I$  is the lumped mass for the node  $I$ ,  $f_{Ii}^{\text{ext}}$  and  $f_{Ii}^{\text{int}}$  are equivalent external force and internal force, respectively.

### 2.3.2. Discretization for the heat conduction equation

The heat conduction equation in coupled thermal elastic problems is used to determine the temperature evolution, which considers the effect of bulk strain rate on temperature.

Applying weak form Galerkin variational principle, we can obtain

$$\int_{\Omega} \left[ \delta T^s \left( \rho^s c^s \frac{\partial T^s}{\partial t} \right) + \left( \frac{\partial \delta T^s}{\partial x_j} \right) \left( k^s \bar{T}_j^s \right) - \delta T^s Q + \delta T^s \beta^s (\dot{\epsilon}_v) \right] d\Omega - \int_{\Gamma_2} \delta T^s q d\Gamma - \int_{\Gamma_3} \delta T^s h (T_{\infty}^s - T^s) d\Gamma = 0, \quad (22)$$

where  $T_{\infty}^s$  is the ambient temperature,  $q$  is the prescribed heat flux,  $h$  is the heat convection coefficient. Using the shape function of polynomial interpolation, Eq.(17) can be re-written as

$$\int_{\Omega} \left[ \left( \rho^s c^s N_I N_J \frac{\partial T^s}{\partial t} \right) + \overline{\left( \frac{\partial N_I}{\partial x_j} \right)} \left( \frac{\partial N_J}{\partial x_j} \right) \left( k^s \bar{T}_j^s \right) - N_I Q + N_I \beta^s T_0^s (\dot{\epsilon}_v) \right] d\Omega - \int_{\Gamma_2} N_I q d\Gamma - \int_{\Gamma_3} N_I h (T_{\infty}^s - N_J T_J^s) d\Gamma = 0, \quad (23)$$

Finally, ES-FEM formulations for heat conduction equation are given as

$$C_{IJ} \dot{T}_J^s + K_{IJ} T_J^s = P_I, \quad (24)$$

$$C_{IJ} = \int_{\Omega} \rho^s c^s N_I N_J d\Omega, \quad (25)$$

$$K_{IJ} = \int_{\Omega} \left( k^s \left( \frac{\partial N_I}{\partial x^{\alpha}} \right) \left( \frac{\partial N_J}{\partial x^{\alpha}} \right) \right) d\Omega + \int_{\Gamma_3} h N_I N_J d\Gamma, \quad (26)$$

$$P_I = P_{Q_I} + P_{q_I} + P_{H_I} + P_{\dot{\epsilon}_v I}, \quad (27)$$

$$P_{Q_I} = \int_{\Omega} Q N_I d\Omega, \quad (28)$$

$$P_{q_I} = \int_{\Gamma_2} q N_I d\Gamma, \quad (29)$$

$$P_{H_I} = \int_{\Gamma_3} h T_{\infty} N_I d\Gamma, \quad (30)$$

$$P_{\dot{\epsilon}_v I} = - \int_{\Omega} \beta^s T_0^s (\dot{\epsilon}_v) N_I d\Omega, \quad (31)$$

where  $C_{IJ}$  is the heat capacity matrix,  $K_{IJ}$  is the heat conduction matrix,  $P_I$  is the temperature load matrix,  $P_{Q_I}$  is temperature load from body heat source,  $P_{q_I}$  is the temperature load from heat flux boundary,  $P_{H_I}$  is temperature load from heat convection boundary,  $P_{\dot{e}_v I}$  is temperature load from thermo-elastic heating. In addition, the lumped mass heat capacity matrix is used.

In this paper, the staggered solution strategy is adopted for fully coupled thermal elastic problems. In each time step, the mechanical results of the previous time step are applied to solve the thermal part, and then the thermal results of the current time step is used to solve the mechanical part. Moreover, the transient solutions of the fully coupled thermal elastic problems are achieved applying the explicit time integration based on the central difference algorithm.

### 3. SPH formulations for thermal-fluid flows

#### 3.1. Governing equations

Recently, thermal fluid flows have been simulated successfully using the weakly compressible SPH (WCSPH) method [72–74]. In these WCSPH models, the Boussinesq's approximation is applied. Moreover, the compressibility term and viscous dissipation term in energy equation are small enough to be neglected. In this article, the incompressible and Newtonian fluid is considered. The WCSPH is applied for modeling incompressible fluid flows. Then, the incompressible fluid is assumed to be slightly or weakly compressible. The conservation equations of coupled mass, momentum and energy are given as

$$\frac{d\rho}{dt} + \rho \frac{\partial v_i}{\partial x_i} = 0, \quad (32)$$

$$\frac{dv_i}{dt} = -\frac{1}{\rho} \frac{\partial p}{\partial x_i} + v_0 v_{i,jj} + b_i, \quad (33)$$

$$\frac{dT}{dt} = \frac{k^f}{\rho c} T_{,ii}, \quad (34)$$

where  $\rho$  is the density of fluid,  $x_i$  and  $v_i$  is the spatial position and velocity of fluid, respectively.  $p$  is the pressure,  $v_o$  is the kinematic viscosity of fluid,  $b_i$  is the body force of fluid,  $T$ ,  $k^f$ ,  $c$  are the absolute temperature, the coefficient of thermal conductivity and specific heat of fluid, respectively. Boussinesq approximation is utilized for calculating the body force, the expression of body force is written as

$$b_i = \alpha_T^f (T - T_0^f) g_i, \quad (35)$$

where  $\alpha_T^f$  is the thermal expansion coefficient of fluid,  $g_i$  is acceleration of gravity.

#### 3.2. SPH approximations

The SPH method is a purely Lagrangian meshless approach to solve partial differential equations, which is based on integral interpolants. In SPH, the fluid domain is discretized into a group of particles, where all the relevant physical quantities are approximated according to the integral representation over adjacent particles. The SPH approximations for field function  $f(\mathbf{x}^a)$  and its derivative  $\frac{\partial f(\mathbf{x}^a)}{\partial x_i}$  at position  $\mathbf{x}^a$  can be obtained as [53,75]

$$f(\mathbf{x}^a) = \sum_b \frac{m^b}{\rho^b} f(\mathbf{x}^b) W^{ab}, \quad (36)$$

$$\frac{\partial f(\mathbf{x}^a)}{\partial x_i} = \sum_b \frac{m^b}{\rho^b} f(\mathbf{x}^b) \frac{\partial W^{ab}}{\partial x_i}, \quad (37)$$

where subscript  $a$  and  $b$  are particle indices,  $m$  is the mass,  $W$  is a kernel function, and cubic spline kernel function [76] is adopted in this article.

#### 3.3. Discretization equations

Applying the SPH concepts expressed in Eq. (32), discretization of continuity Eq. (32) can be written as

$$\frac{d\rho^a}{dt} = \rho^a \sum_b \frac{m^b}{\rho^b} (v_i^a - v_i^b) \frac{\partial W^{ab}}{\partial x_i^a}, \quad (38)$$

where  $v_i^a$  is the velocity of particle  $a$ ,  $x_i^a$  is the spatial position of particle  $a$ ,  $m^a$  and  $\rho^a$  is the mass and density of particle  $a$ , respectively.

The Laminar viscosity is utilized in this paper, the discrete form of Laminar viscous term suggested by Morris [77] is used, which is given as

$$(v_o \nabla^2 v_i)_a = \sum_b \frac{4m^b v_o x_j^{ab} (\partial W^{ab} / \partial x_j^a)}{(\rho^a + \rho^b)(x_k^{ab} x_k^{ab} + \eta^2)} v_i^{ab}, \quad (39)$$

where  $x_j^{ab} = x_j^a - x_j^b$  and  $v_i^{ab} = v_i^a - v_i^b$  are the relative position and velocity of particles, respectively.  $\eta = 0.1 h_{sml}$  is a parameter used to avoid the null denominator, and  $h_{sml}$  is smooth length. Then, the discretization of momentum conservation equation can be written as

$$\frac{dv_i^a}{dt} = - \sum_b m^b \left( \frac{p^a}{(\rho^a)^2} + \frac{p^b}{(\rho^b)^2} \right) \frac{\partial W^{ab}}{\partial x_i^a} + \sum_b \frac{4m^b v_o x_j^{ab} (\partial W^{ab} / \partial x_j^a)}{(\rho^a + \rho^b)(x_k^{ab} x_k^{ab} + \eta^2)} v_i^{ab} + b_i. \quad (40)$$

Applying the SPH concepts expressed in Eq. (34), discretization of energy Eq. (34) can be written as

$$\frac{dT^a}{dt} = \frac{1}{\rho^a c^a} \sum_b \frac{4m^b (k^f)^a (k^f)^b}{\rho^a \rho^b ((k^f)^a + (k^f)^b)} (T^a - T^b) \frac{x_i^{ab} (\partial W^{ab} / \partial x_i^a)}{(x_j^{ab} x_j^{ab} + \eta^2)}. \quad (41)$$

In addition, the pressure is computed by EOS [78], and the expression is given as follows

$$p = c_{ns}^2 (\rho - \rho_0), \quad (42)$$

where  $\rho_0$  is a reference density,  $c_{ns}^2$  is a numerical speed of sound.

#### 3.4. Enhancement of sph

In this paper, the particle shifting technique (PST) and kernel gradient correction (KGC) are integrated into the conventional SPH method to improve the computational accuracy and stability of SPH. The particle shifting technique (PST) proposed by Xu et al. [79] is applied to avoid disordered particle distributions. Lind et al. [80] proposed a generalized version of PST and extended application to free surface flows. Recently, Khayyer et al. [81] developed an optimized PST that can obtain better results when simulating of free-surface or multiphase flows. However, these PST models are valid for the particles with the equal scale, whereas it should be changed if particles with different scale are utilized. As the size of ghost particles is much less than the size of real fluid particles (detailed description in Section 4), a modified particle shifting vector [59] is applied in this paper, the expression is

$$\delta x_i^a = \beta \sum_b \frac{x_i^{ab}}{\left| \sqrt{x_j^{ab} x_j^{ab}} \right|^3} r_o^2 \frac{m^b}{m^a} U_{\max} \Delta t, \quad (43)$$

and

$$r_o = \sum_{b=1}^{N_f} \left| \sqrt{x_j^{ab} x_j^{ab}} \right| / N_f, \quad (44)$$

where  $\delta x_i^a$  is the shifting vector of the particle  $a$ ,  $\beta$  is a free parameter that can be changed depending on each problem,  $r_o$  is the mean particle distance, and  $N_f$  is the number of neighboring fluid particles.

A kernel gradient correction (KGC) technique [82] is utilized to improve the computational accuracy. In the KGC approach, a corrected

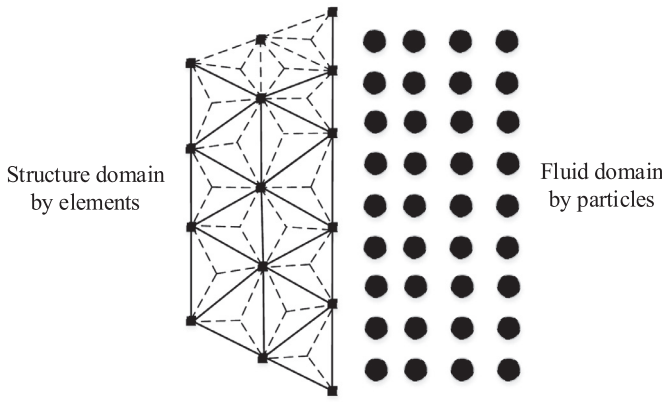


**Fig. 2.** Illustration of interface between structure elements and fluid particles.

kernel derivative  $\left[\frac{\partial W^{ab}}{\partial x_i^a}\right]^C$  is obtained from Taylor series expansion approach. In 2D spaces, the modified kernel derivative  $\left[\frac{\partial W^{ab}}{\partial x_i^a}\right]^C$  can be obtained as follows

$$\left[\frac{\partial W^{ab}}{\partial x_i^a}\right]^C = L_{ij}^a \frac{\partial W^{ab}}{\partial x_j^a}, \quad (45)$$

$$L_{ij}^a = \left(M_{ij}^a\right)^{-1}, \quad (46)$$

$$M_{ij}^a = \sum_b \frac{m^b}{\rho^b} x_j^b \frac{\partial W^{ab}}{\partial x_i^a}. \quad (47)$$

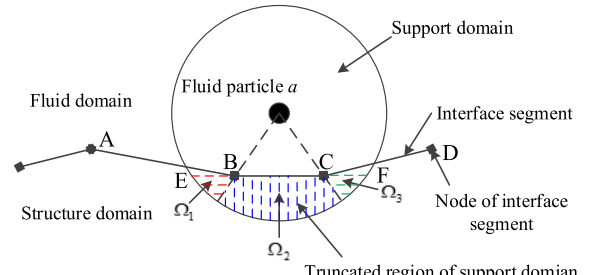
#### 4. Ghost particle coupling algorithm

In this work, the ES-FEM-SPH coupling approach is developed for TFSI problems. As shown in the Fig. 2, the ES-FEM is applied for solving coupled thermal elastic problem of structure domain and the SPH approach is applied for solving thermal convection of fluid domain. For treatment of the thermal fluid structure interface, the kinematic condition and dynamics condition should be satisfied for fluid structure interaction, and the continuity condition of temperature and conservation of energy should be satisfied for fluid structure conjugate heat transfer. Then, the coupling approach involves two treatments for treating thermal fluid structure interface. One is the ghost coupling algorithm for treating fluid structure interaction, the other is the ghost coupling algorithm for treating fluid structure conjugate heat transfer.

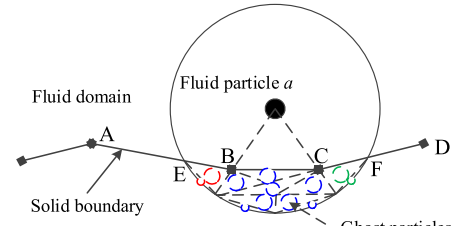
##### 4.1. Treatment of fluid-structure interaction

In this work, the coupling algorithm based on ghost particles developed by Long et al. [59] is applied for fluid structure interaction. When a fluid particle moves near the interface, the support domain of the particle is cut off by interface segment of elements region. In order to repair the support domain of the particle, the ghost particles are generated by separating the truncated region of support domain. In order to facilitate the establishment of the interaction pair between an element and a particle, the truncated region is separated into subareas according to interface segment. As illustrated in Fig. 3(a), the truncated area is separated into subareas of  $\Omega_1, \Omega_2$  and  $\Omega_3$ , in which  $\Omega_1, \Omega_2$  and  $\Omega_3$  correspond with the interface segment of AB, BC and CD, respectively. Then, the ghost particles can be generated by separating the subareas as illustrated in Fig. 3(b). The physical quantities of ghost particles are obtained through interpolation based on boundary condition. During each time step, the ghost particles are created automatically. Furthermore, the moving boundaries with complex geometry can be easily handled.

The interaction pairs between fluid particles and interface segments should be recognized at first, and the method proposed by Long et al. [59] is applied. After interaction pairs have been determined, the ghost



(a) Dividing truncated area into subareas



(b) Ghost particles generated by discretizing subareas

**Fig. 3.** Dividing truncated area into subareas and producing ghost particles.

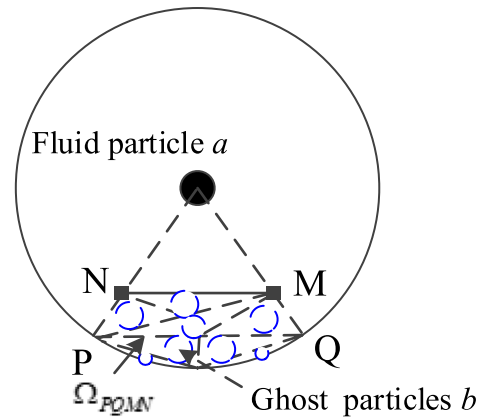


**Fig. 4.** Fluid particle  $a$  interacts with interface segment  $MN$  through ghost particles.

particles are produced for each interaction pair. Then, the interaction force between interface segment and particle can be calculated through the ghost particles. As illustrated in the Fig. 4, the interface segment  $MN$  interacts with the fluid particle  $a$  and the ghost particles are generated by discretizing the corresponding subarea  $\Omega_{MNPQ}$ . The force  $f_i^{S_{MN}tF_a}$  of the interface segment  $MN$  acting on fluid particle  $a$  is given as

$$f_i^{S_{MN}tF_a} = \sum_b f_i^{G_b tF_a} = m^a \left[ - \sum_b m^b \left( \frac{p^a}{(\rho^a)^2} + \frac{p^b}{(\rho^b)^2} \right) \frac{\partial W^{ab}}{\partial x_i^a} \right. \\ \left. + \sum_b \frac{m^b (v_o^a + v_o^b) x_j^b (\partial W^{ab} / \partial x_j^a)}{\rho^b (x_k^a x_k^b + \eta^2)} v_i^{ab} \right], \quad (48)$$

where  $f_i^{S_{MN}tF_a}$  denotes the force of segment  $MN$  applying on the fluid particle  $a$ ,  $f_i^{G_b tF_a}$  denotes the force of the ghost particle  $b$  acting on the fluid particle  $a$ .  $N^\Omega$  is the number of the ghost particles in subarea  $\Omega_{MNPQ}$ .

The opposite forces from the fluid particle  $a$  to the segment  $MN$  is

$$f_i^{F_a t S_{MN}} = -f_i^{S_{MN}tF_a}, \quad (49)$$

and  $f_i^{F_a t S_{MN}}/2$  is exerted on node  $N$  and node  $M$ , respectively.

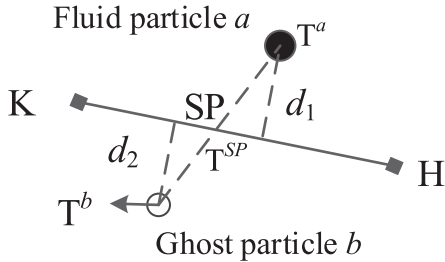


Fig. 5. Temperature of a ghost particle.

#### 4.2. Treatment of fluid structure conjugate heat transfer

In this work, the ghost particle coupling algorithm for fluid structure conjugate heat transfer is developed. The ghost particles and interaction pairs are the same of those used for fluid structure interaction. The temperature of ghost particle is obtained based on continuity condition of temperature. As illustrated in Fig. 5, the temperature of a ghost particle  $b$  can be obtained as

$$T^b = T^{SP} + (T^{SP} - T^a) \frac{d_2}{d_1}, \quad (50)$$

where  $T^{SP}$  denotes the temperature of the point SP in segment KH,  $d_1$  and  $d_2$  are the vertical distance of the fluid particle  $a$  and the ghost particle  $b$  to the segment KH, respectively.

For calculating the temperature of particle  $a$ , both the real and ghost particles are included in the sums of energy equation. When ghost particles are added, energy equation for SPH becomes

$$\frac{dT^a}{dt} = \frac{1}{\rho^a c^a} \sum_b^{N^r + N^g} \frac{4m^b (k^f)^a (k^f)^b}{\rho^a \rho^b ((k^f)^a + (k^f)^b)} (T^a - T^b) \frac{x_i^{ab} (\partial W^{ab} / \partial x_i^a)}{(x_j^{ab} x_j^{ab} r + \eta^2)}, \quad (51)$$

where  $N^g$  and  $N^r$  are the number of ghost and real particles in the influence domain of particle  $a$ , respectively.

As shown in the Fig. 4, the heat flow rate from the segment MN to fluid particle  $a$  is given as

$$Q^{MN\_t\_a} = \frac{m^a}{\rho^a} \sum_b^{N^{\Omega}} \frac{4m^b (k^f)^a (k^f)^b}{\rho^a \rho^b ((k^f)^a + (k^f)^b)} (T^a - T^b) \frac{x_i^{ab} (\partial W^{ab} / \partial x_i^a)}{(x_j^{ab} x_j^{ab} r + \eta^2)}, \quad (52)$$

where  $Q^{MN\_t\_a}$  denotes the heat flow rate from segment MN to fluid particle  $a$ . According to conservation of energy, the heat flux from the particle  $a$  to element boundary segment MN is given as

$$q^{a\_t\_MN} = -\frac{Q^{MN\_t\_a}}{l^{MN}}, \quad (53)$$

where  $q^{a\_t\_MN}$  denotes the heat flux from the particle  $a$  to element boundary segment MN,  $l^{MN}$  is the length of segment NM. Then, the heat flux  $q^{seg\_MN}$  of segment MN is given as

$$q^{seg\_MN} = \sum_a^{N^{a\_t\_MN}} q^{a\_t\_MN}, \quad (54)$$

where  $N^{a\_t\_MN}$  is the total number of fluid particles interacting with the segment MN.

Appling the heat flux boundary condition on segment MN for ES-FEM, the temperature load is given as

$$P_{qI}^{seg\_NM} = \int_{\Gamma_{MN}} q_{seg\_MN} N_I d\Gamma, \quad (55)$$

where  $P_{qI}^{seg\_NM}$  is the temperature load from contribution of interface segment MN.

With the use of the ghost particle coupling algorithm, the kinematic condition, dynamics conditions and conservation of energy are satisfied.

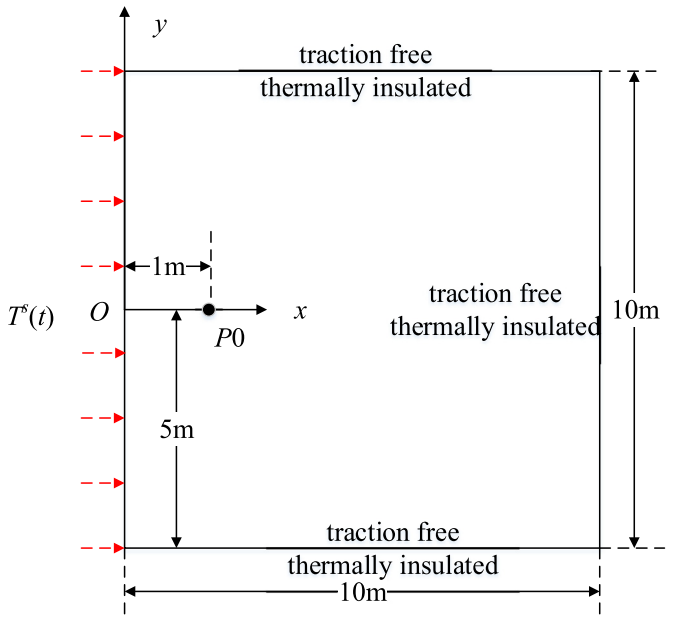


Fig. 6. A square plate subjected to thermal loading.

The velocities of ghost particles are obtained according to continuity condition of velocity to make sure satisfy the kinematic condition. The interaction force between interface segment and particle is calculated through the ghost particles, and the forces from structure to fluid are equal in magnitude to the forces from fluid to structure. Thus, dynamic conditions is satisfied and the virtual work of fluid load and solid force on the interface displacement is equal. Moreover, the thermal energy absorbed by structure is equal to the thermal energy released by fluid. As such, the energy conservation is satisfied.

## 5. Numerical examples

In this section, four benchmark examples are used to verify the effectiveness of present coupling approach for modeling TFSI problems. The first example is coupled thermal elastic problem of a half-space to verify the developed ES-FEM for coupled thermal elastic problems. The second case is natural convection in a square cavity to verify the present SPH method for thermal fluid flows. The third case is the heat convection in a square cavity with a stiffness plate to verify the ghost particle coupling algorithm for treating fluid structure conjugate heat transfer. The last case is a fully thermal-fluid-structure interaction problem, which involves thermal convection in a square cavity with a flexible beam to verify the developed ES-FEM-SPH coupling approach for TFSI problem.

### 5.1. Example I: coupled thermal elastic problem of a half-space

In order to verify the effectiveness of ES-FEM for thermal elastic problems, coupled thermal elastic problem of a half-space is considered. In order to simulate the half space model under thermal shock, a similar model of a square plate subjected to heating at left edge with a step function for temperature rise is considered, as shown in Fig. 6. The plate is thermally isolated and is traction free at the other three edges. The results are obtained at point P0 located at (1, 5) of the plate. The plane strain assumption is adopted for the problem, and the boundary element method (BEM) solution and analytical solution are given by Chen and Dargush [83] and Sternberg and Chakravorty [84], respectively.

The step function for temperature is given as

$$T^s(t) = T_h^s H(t) + T_0^s, \quad (56)$$

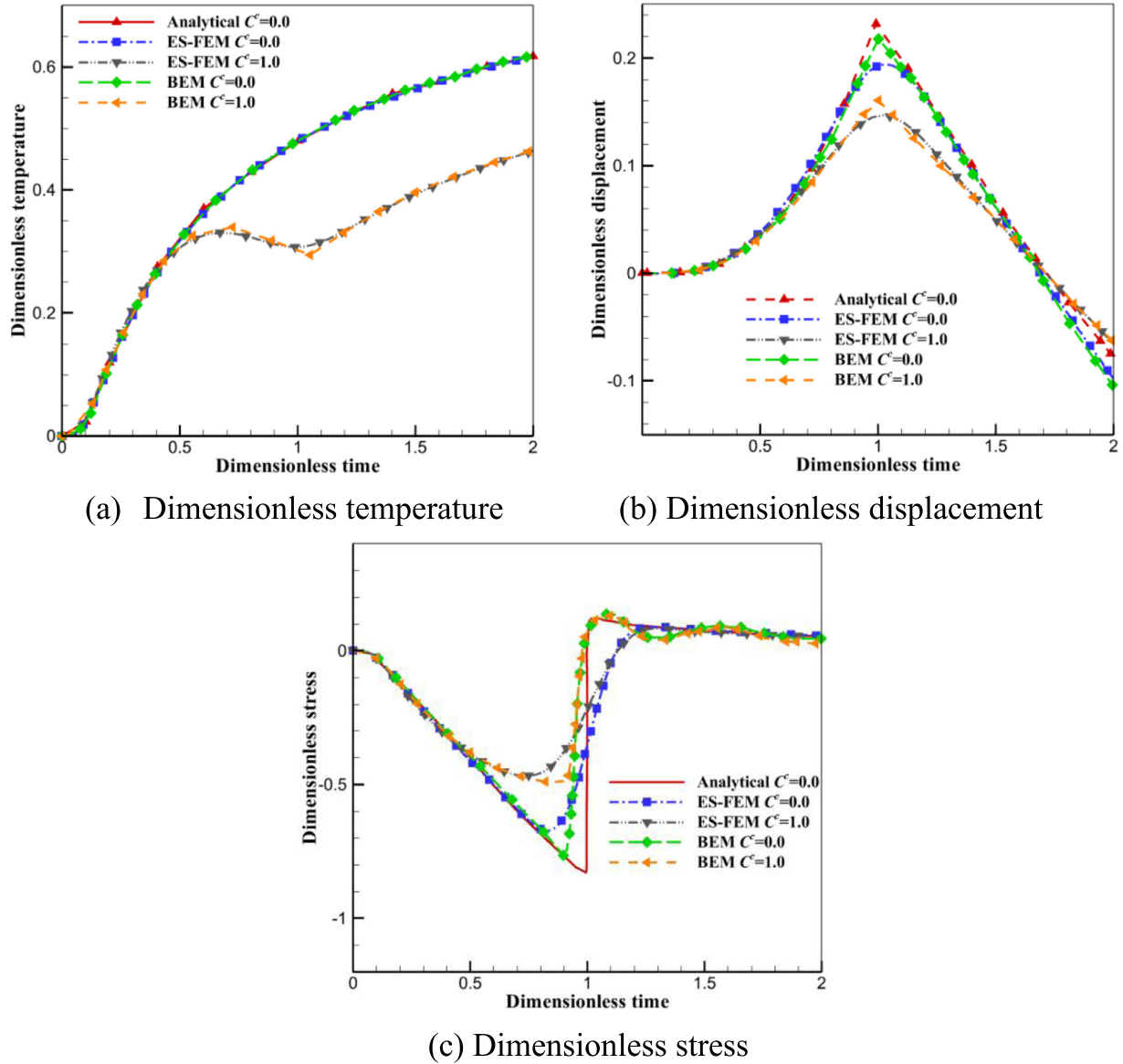


Fig. 7. Time history of dimensionless temperature, displacement and stress at point P0.

where  $T_h^s$  is the amplitude,  $H(t)$  is unit step function, the expression is written as

$$H(t) = \begin{cases} 1 & t > 0 \\ 0 & t \leq 0 \end{cases}. \quad (57)$$

To facilitate comparison of results, the dimensionless variables are given as follows

$$\hat{x}_i^s = \frac{x_i^s}{\chi}, \quad \hat{t} = \frac{C^1}{\chi}t, \quad \hat{T}^s = \frac{T^s - T_0^s}{T_h^s}, \quad (58)$$

$$\hat{u}_i^s = \frac{\lambda + 2\mu}{\chi\beta^s T_h^s} u_i^s, \quad \hat{\sigma}_{ij} = \frac{1}{\beta^s T_h^s} \sigma_{ij}, \quad (59)$$

Where  $\chi$  and  $C^1$  are dimensionless characteristic length and propagation velocity of longitudinal elastic stress wave, respectively, defined as

$$\chi = \frac{k^s}{\rho^s c^s C^1}, \quad (60)$$

$$C^1 = \sqrt{\frac{\lambda + 2\mu}{\rho^s}}. \quad (61)$$

Table 1  
Material properties of plate in Example I.

Material properties	Value
Density $\rho^s$	1Kg/m <sup>3</sup>
Heat capacity $c^s$	1J/(KgK)
Heat conductivity $k^s$	1W/(m <sup>2</sup> K)
Elastic modulus $E$	0.743 Pa
Poisson's ratio $\nu$	0.3
Thermal expansion coefficient $\alpha_T$	0.538/K

The coupled amplitude of temperature and deformation field is given by coupling parameter  $C^c$ , and it can be written as

$$C^c = \frac{T_0^s(\beta^s)^2}{\rho^s c^s (\lambda + 2\mu)}. \quad (62)$$

Dimensionless variables are calculated by selecting material properties, Table 1 shows the material properties used in this work. In addition,  $T_h^s = 0.0001$  is utilized in this article.

Fig. 7 show the dimensionless time history of dimensionless temperature  $\hat{T}^s$ , dimensionless  $x$ -direction displacement  $\hat{u}_x^s$ , dimensionless

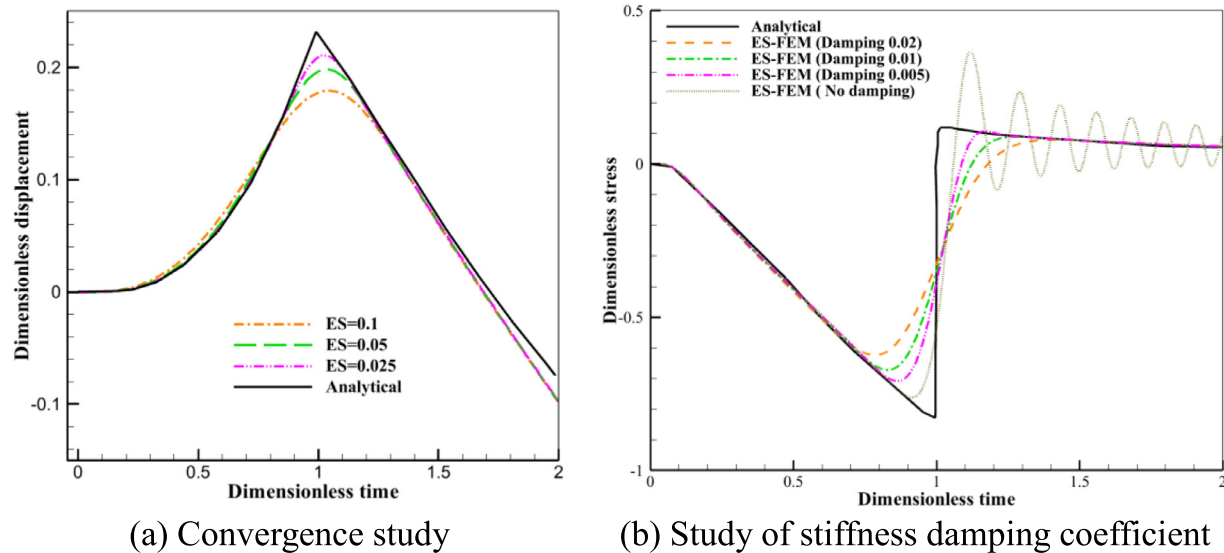


**Fig. 8.** Study of convergence study (ES denotes element spacing) and stiffness damping coefficient.

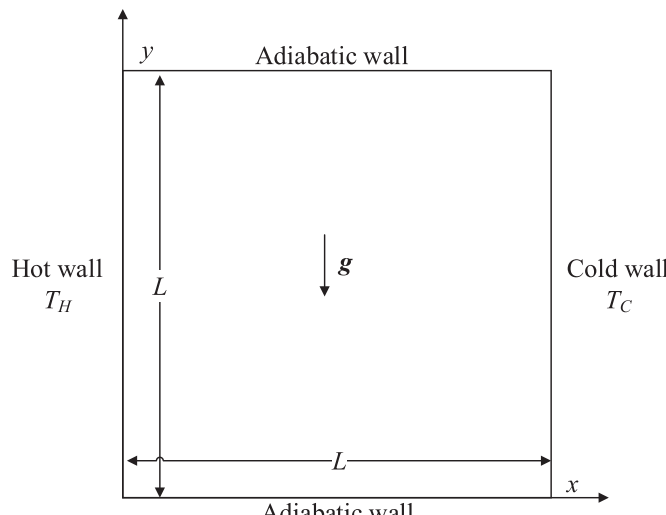


**Fig. 10.** Natural convection in a square cavity.

horizontal stress  $\hat{\sigma}_{xx}$  at point P0, and the results for two different coupling parameters  $C^c$  (0 and 1) have been considered. The value of  $C^c = 0$  and  $C^c = 1$  indicates the uncoupled and strong coupling solution, respectively. The results obtained by ES-FEM are in good agreement with boundary element solution [83] and analytical solution [84]. As shown in the Fig. 7(a), the coupling parameter affects the amplitude of temperature and the influence becomes obvious after dimensionless time  $\hat{t} = 0.5$ . The value of propagation velocity of longitudinal elastic wave is  $C^1 = 1$ . Then, the wave front will reach point P0 ( $\hat{x}_x^s = 1$ ) at time  $\hat{t} = 1.0$ . As shown in the Fig. 7(b), the peak value of dimensionless displacement appears at time  $\hat{t} = 1.0$ , and then moves in the opposite direction. Fig. 7(c) illustrates that the maximum magnitude of horizontal stress obtained by strong coupling is lower than those obtained by uncoupled.

Moreover, the influence of element resolution on ES-FEM model is studied, as shown in the Fig. 8(a), the abbreviation ES denotes the mesh spacing. The dimensionless displacement obtained by ES-FEM is closer to analytical solution with the decrease of mesh spacing. In addition, the stiffness damping is used in this example and the expression is given

as

$$f_{II}^{damp} = \beta^{damp} \int_{\Omega} \frac{\partial N_I}{\partial x_i} \overline{\sigma_{ji}} d\Omega, \quad (63)$$

where  $f_{ii}^{damp}$  is stiffness damping force,  $\rho^{damp}$  is the damping coefficient,  $\dot{\sigma}_{ji}$  is smoothed Cauchy stress rate. Fig. 8(b) shows the influence of stiffness damping force, the stress will oscillate without stiffness damping force.

Fig. 9 shows the distribution of dimensionless horizontal stress and displacement at dimensionless time  $\hat{t} = 1.0$ , respectively. It is clear that the stress and temperature field are smooth and correct. The results of this example indicate that the ES-FEM developed in this paper is effective for modeling coupled thermal elastic problems.

## 5.2. Example II: natural convection in a square cavity

The natural convection in a square cavity is used to verify the effectiveness of SPH method for thermal fluid flows. As illustrated in Fig. 10, the length of closed square is  $L = 10\text{m}$ . Initially, the fluid is at rest with temperature  $T_0^f = 600\text{K}$ . At the beginning, the left side wall is suddenly heated to  $T_H = 1100\text{K}$  and then remains unchanged. The right wall is suddenly cooled to  $T_C = 100\text{K}$  and then remains unchanged. Moreover, the adiabatic wall boundary condition is utilized for bottom and top wall, and No-slip boundary condition is used for all boundaries. The dimensionless parameters of Prandtl number  $Pr$  and Rayleigh number  $Ra$  are utilized in this paper, the expressions are given as

$$Pr = \frac{v_0 \rho c}{k^f}, \quad (64)$$

$$Ra = \frac{g\alpha_T^f L^3 (T_H - T_C) \rho c}{v_0 k^f}. \quad (65)$$

In this example,  $Pr = 0.71$  and  $Ra = 10^6$  are used, and the other parameters of simulation are shown in Table 2.

**Fig. 11(a)** and **Fig. 11(b)** show the horizontal and vertical velocity profiles along the central lines  $x/L = 0.5$  and  $y/L = 0.5$ , respectively. It can be seen that the results obtained by present SPH method are in good agreement with bench mark solution by Wan et al. [85]. **Fig. 11(c)** shows the Nusselt number  $Nu$  along the cold, the Nusselt number is defined as

$$Nu|_{\text{wall}} = \frac{L}{T_H - T_C} \left| \frac{\partial T}{\partial x} \right|_{\text{wall}}. \quad (66)$$

The result obtain by present SPH agree well with the reference solution by Wan et al. [85]. Moreover, the fields of pressure, velocity and

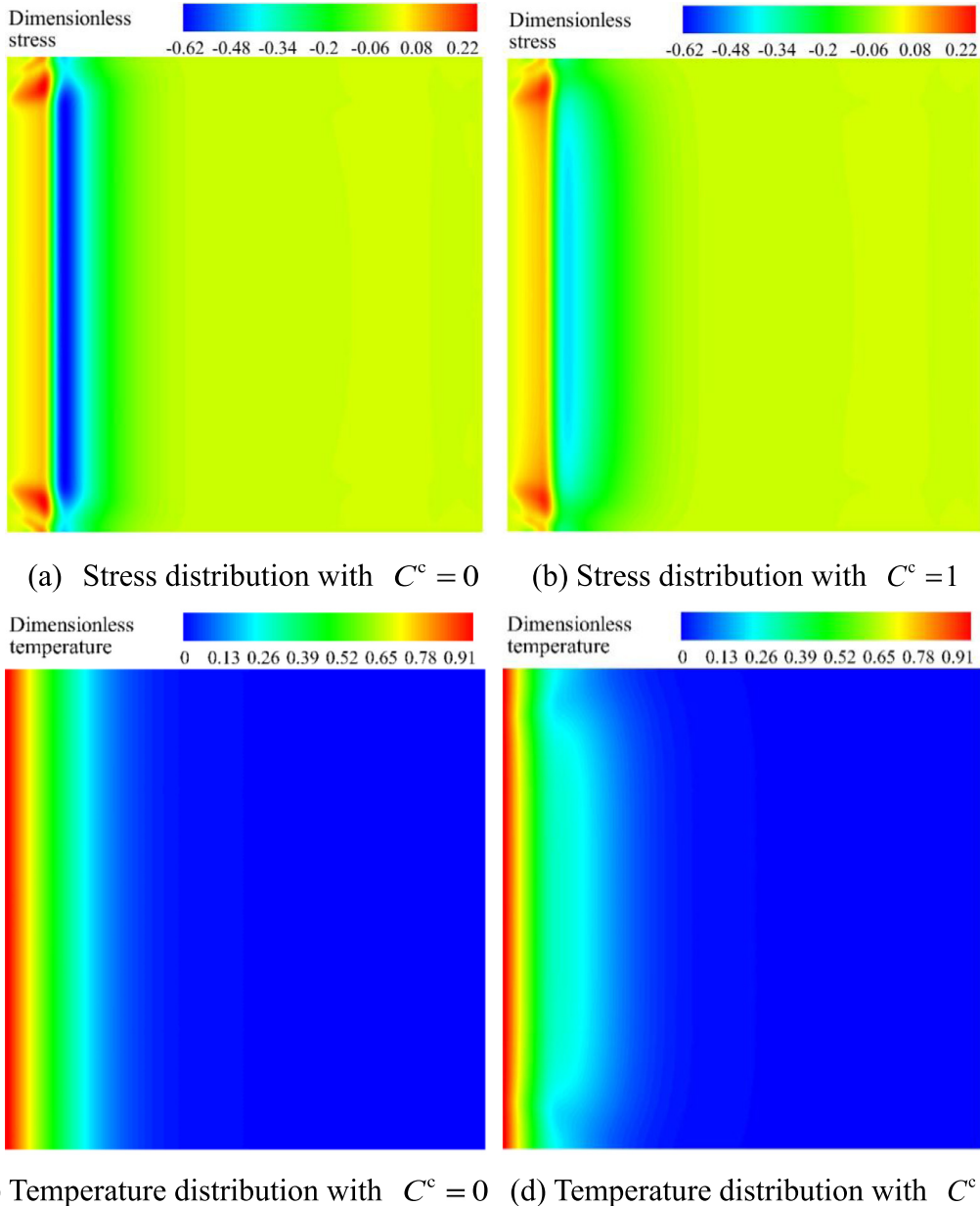


**Fig. 9.** Distribution of dimensionless horizontal stress and temperature at dimensionless time  $\hat{t} = 1.0$ .

**Table 2**  
Parameters of simulation in Example II.

Parameters	Value
Density $\rho$	1Kg/m <sup>3</sup>
Heat capacity $c$	1J/(KgK)
Heat conductivity $k^f$	1W/(mK)
Thermal expansion coefficient $\alpha_T^f$	0.071/K
Acceleration of gravity $g$	10 m/s <sup>2</sup>
Kinematic viscosity $\nu_0$	0.71m <sup>2</sup> /s

temperature are shown in the Fig. 12 and the results obtained by present SPH method are correct and smoothed. It indicates that the present SPH method integrated with KGC and PST techniques is effective for simulating thermal fluid flows.

### 5.3. Example III: convection in a square cavity with a stiffness plate

The case is the problem of convection in a square cavity with a stiffness plate, and it is used to validate the effectiveness of ghost particle coupling scheme for fluid structure conjugate heat transfer. As shown in the Fig. 13, the stiffness square plate with length of  $d = 4$  m is located in the center of square cavity with length of  $L = 10$  m. Initially, fluid particles in the cavity are motionless and isothermal at a low temperature of  $T_l = 1000\text{K}$ , while the elements of plate are isothermal at a high temperature  $T_h = 2000\text{K}$ . Moreover, the stiffness plate remains fixed without movement and deformation. The fluid structure conjugate heat transfer condition is used for treating interface between fluid and stiffness plate, and the surrounding walls of cavity are adiabatic boundary conditions. No slip boundary condition is utilized for all walls. Boussinesq approximation is also used in this case. The relevant parameter settings of fluid and solid are shown in the Table 3. The solid domain is discretized by triangular elements and the fluid domain is discretized by particles for ES-FEM-SPH model. The element spacing is 0.05 m corre-

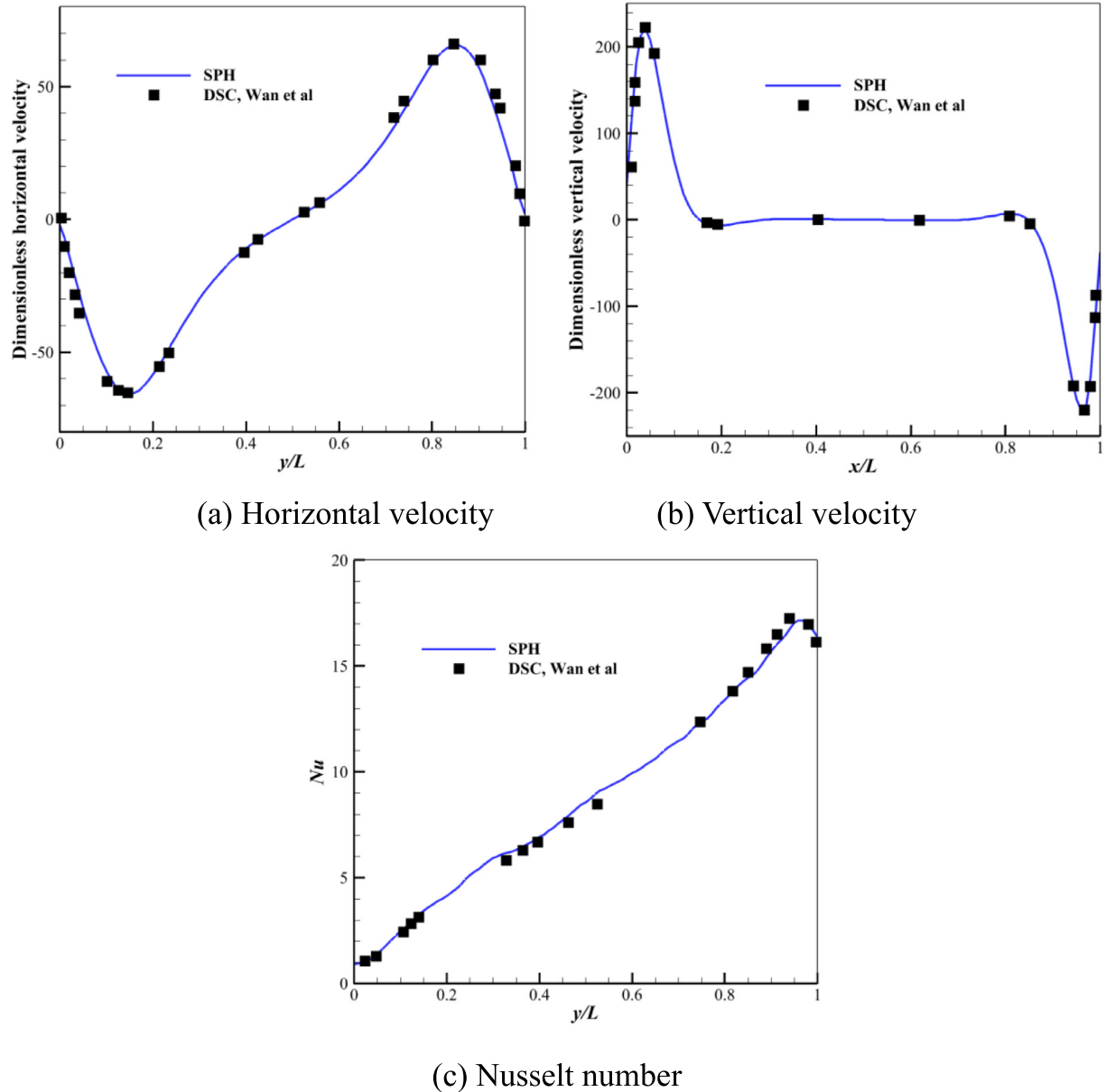


**Fig. 11.** Horizontal and vertical velocity profiles along central lines of cavity and Nusselt number profiles along the cold wall predicted by SPH.

**Table 3**  
Parameters of simulation for conjugate heat transfer  
in Example III.

Parameters	Value
Fluid density $\rho$	1Kg/m <sup>3</sup>
Solid density $\rho^s$	10Kg/m <sup>3</sup>
Fluid heat capacity $c$	1J/(KgK)
Solid heat capacity $c^s$	1J/(KgK)
Fluid heat conductivity $k^f$	1W/(mK)
Solid heat conductivity $k^s$	1W/(mK)
Fluid thermal expansion coefficient $\alpha_T^f$	0.071/K
Acceleration of gravity $g$	10 m/s <sup>2</sup>
Kinematic viscosity $\nu_0$	0.71m <sup>2</sup> /s

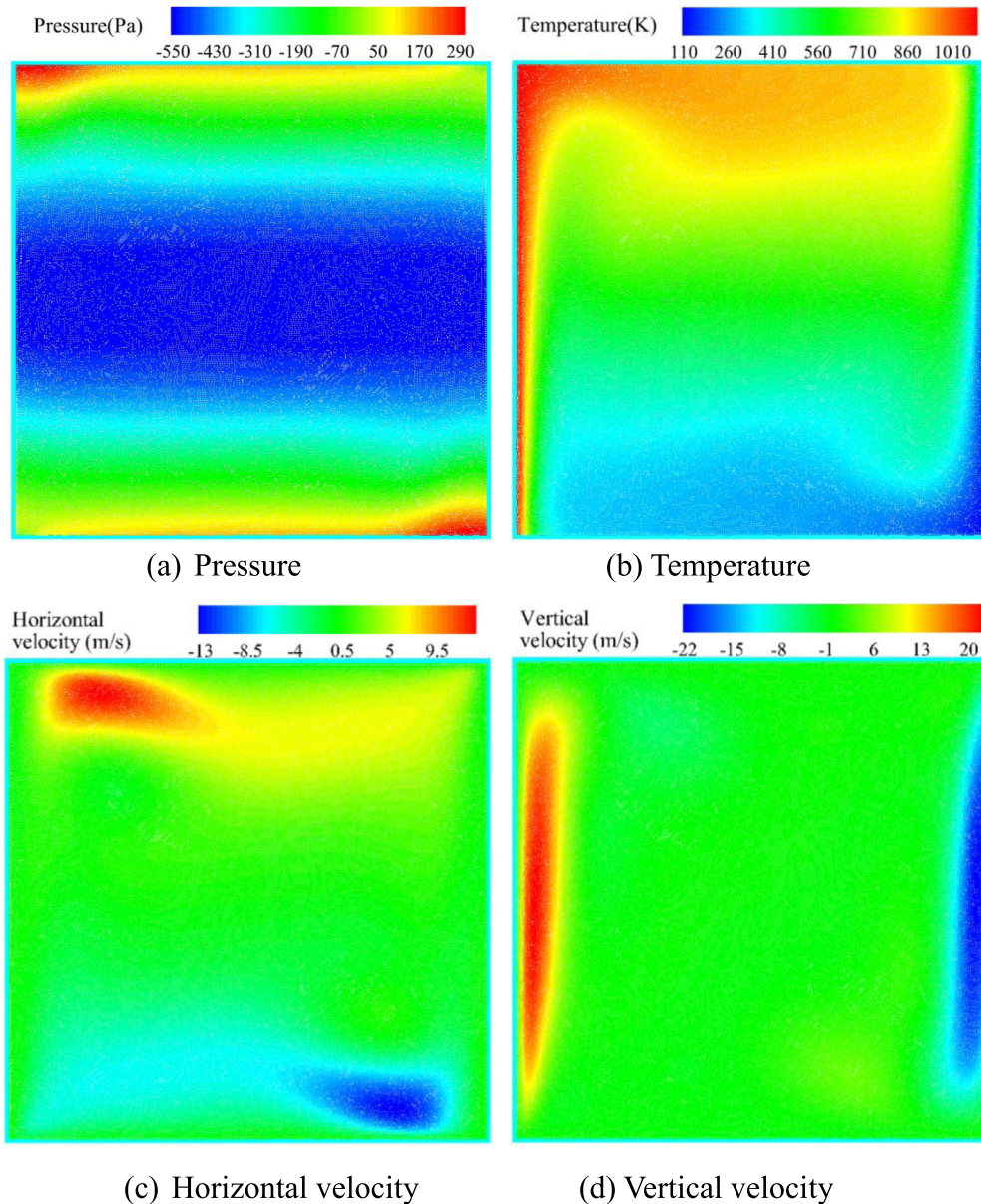
sponding to 14,632 elements for plate, and the particle spacing is 0.05 m corresponding to 33,600 particles. In addition, the case have also been solved by ALE-FEM using COMSOL software. The results obtained by ES-FEM-SPH will be compared with the results of ALE-FEM using COM-

SOL software to verify the accuracy of ghost particle coupling algorithm for fluid structure conjugate heat transfer.

The convergence is studied for ALE-FEM model with 49,014, 82,250, 118,384 and 159,886 triangular elements respectively using COMSOL software. As shown in Fig. 14(a), the results of time history of temperature at point P1 obtained by ALE-FEM model with 118,384 elements are quite close to the results obtained by ALE-FEM model with 159,886 elements, and then the results obtained by ALE-FEM model using 159,886 elements can be utilized as the reference solutions. Fig. 14(b) shows the time history of the temperature at center point P1 of plate, the results obtained by ES-FEM-SPH coupling approach are in good agreement with the results of ALE-FEM using COMSOL software. In order to study on the convergence, the temperature error norm  $L_2$  is defined as

$$L_2 = \sqrt{\frac{1}{N_p + N_e} \left( \sum_{N_p} \left( \frac{T^f - T^{ref}}{T^{ref}} \right)^2 + \sum_{N_e} \left( \frac{T^s - T^{ref}}{T^{ref}} \right)^2 \right)} \quad (67)$$

where  $N_p$  is total number of fluid particles,  $N_e$  is total number of nodes of stiffness plate.  $T^{ref}$  is reference temperature, which is calculated at fine



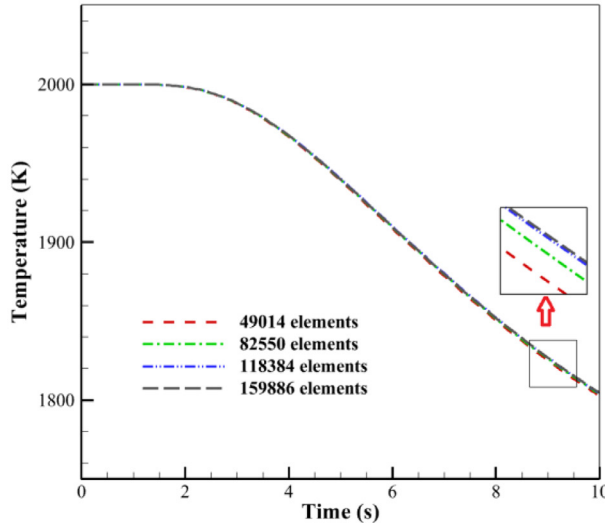
The diagram illustrates a thermodynamic system within a rectangular container. The container has vertical walls labeled "Adiabatic wall" at the top and bottom, and horizontal walls labeled "Adiabatic wall" on the left and right. A coordinate system is established with the origin at the bottom-left corner, where the two adiabatic walls meet. The horizontal axis is labeled  $x$  and the vertical axis is labeled  $y$ . The total width of the container is  $L$ , indicated by a double-headed arrow at the bottom. The total height of the container is  $L$ , indicated by a double-headed arrow on the left. The container contains a central rectangular region with side lengths  $d$ . This central region is divided into two horizontal layers: a lower layer labeled "Solid" with "High temperature" and an upper layer labeled "Fluid" with "Low temperature". A red dot represents a particle located within the solid layer. A dashed vector labeled  $g$  points vertically downwards from the center of the solid layer, representing gravity.

**Fig. 13.** Convection in a square cavity with a stiffness plate.

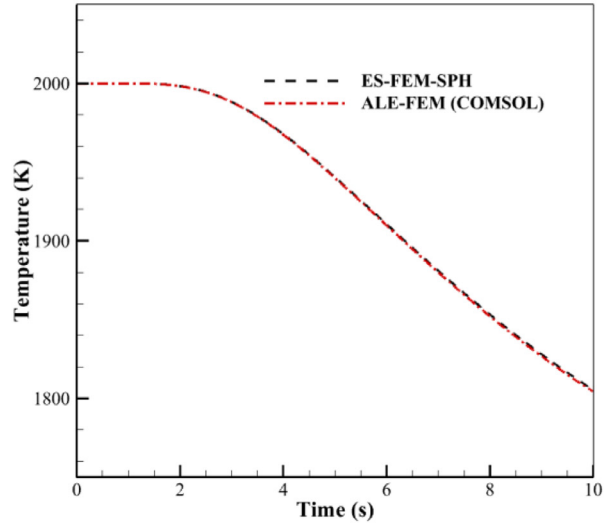
resolution with the element and particle spacing is set to  $\Delta_x = 0.033\text{m}$ . Indeed, the temperature error norm  $L_2$  at time  $t = 5\text{ s}$  is considered. Fig. 15 shows the convergence of temperature error norm at  $t = 5\text{ s}$ , the present ES-FEM-SPH plays good performance in convergence.

As illustrated in Fig. 16, the time histories of the thermal energy absorbed by stiffness plate element and fluid particles at interface of plate and fluid are given out, respectively.  $Q_{s,\text{absorb}}$  and  $Q_{f,\text{absorb}}$  are the thermal energy absorbed by plate element and fluid particles at the interface, respectively. It can be seen that the value of  $Q_{s,\text{absorb}} + Q_{f,\text{absorb}}$  keeps zero all the time, therefore the conservation of energy is satisfied. Fig. 17(a) and Fig. 17(b) show the distributions of temperature at time  $t = 10$  s, the results obtained by ES-FEM-SPH coupling approach agree well with the results of ALE-FEM. And the temperature is continuous at the interface of fluid and structure. Fig. 17(c) and Fig. 17(d) show the magnitude of velocity distribution at time  $t = 10$  s. Fig. 17(e) and Fig. 17(f) show the distributions of pressure at time at time  $t = 10$  s. It can be seen that the results from ES-FEM-SPH are in good agreement with the results from ALE-FEM.

The results of this example indicate that the ghost coupling algorithm for structure fluid conjugate heat transfer is accurate and effective, and

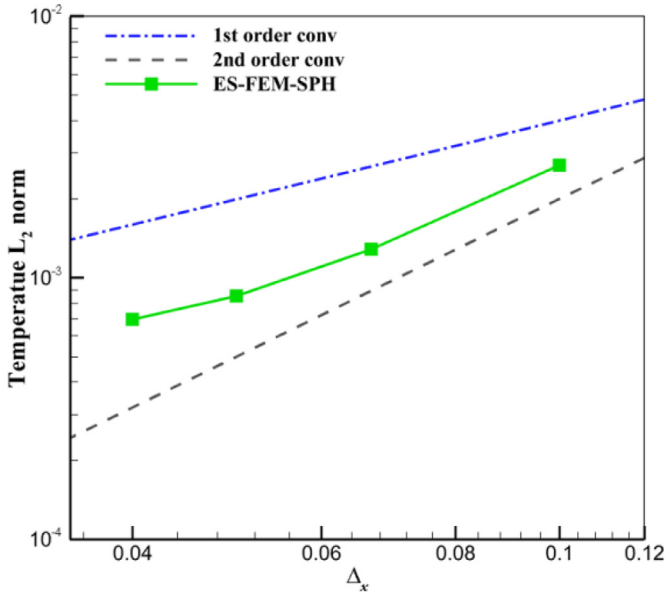


(a) Convergence study



(b) The time history of temperature

Fig. 14. The time history of temperature at central point P1 using COMSOL software and ES-FEM-SPH model.

Fig. 15. Convergence of temperature error L<sub>2</sub> norm.

the continuity of temperature and conservation of energy are satisfied at interface of structure and fluid.

#### 5.4. Example IV: convection in a square cavity with a flexible beam

The case of convection in a two dimensional square cavity with a flexible beam is used to verify the accuracy and effective of the ES-FEM-SPH coupling approach for thermal fluid structure interaction problem. The geometry of the current case is shown in Fig. 18, the side length of the square cavity is  $L = 10$  m. The fluid is filled in the cavity and it is assumed to be incompressible and Newtonian with a Prandtl number of 0.71. Furthermore, the thermal physical properties of the fluid are assumed to be constants except for density variation, which is modeled using the Boussinesq approximation. The length and height of the flexible beam is  $l_1=4$  m and  $h = 0.2$  m, respectively. The bottom left endpoint of rectangle C2 is located at (5, 5), and the left boundary of the flexible beam is fixed. The no-slip conditions are utilized on the flexible beam

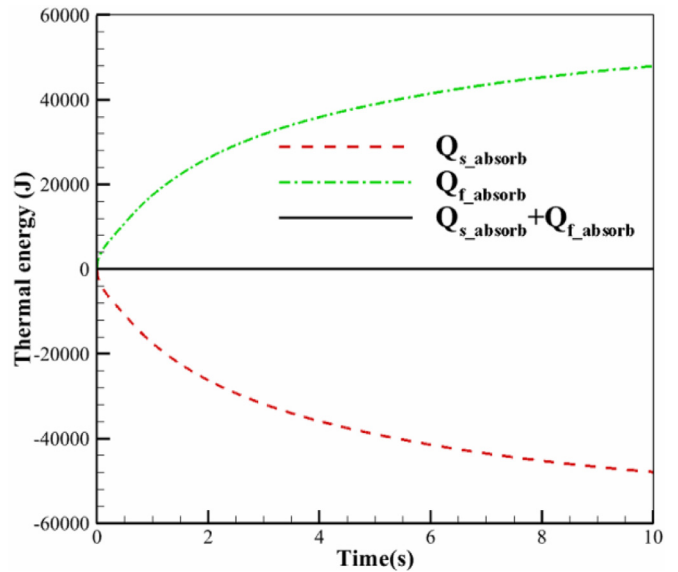
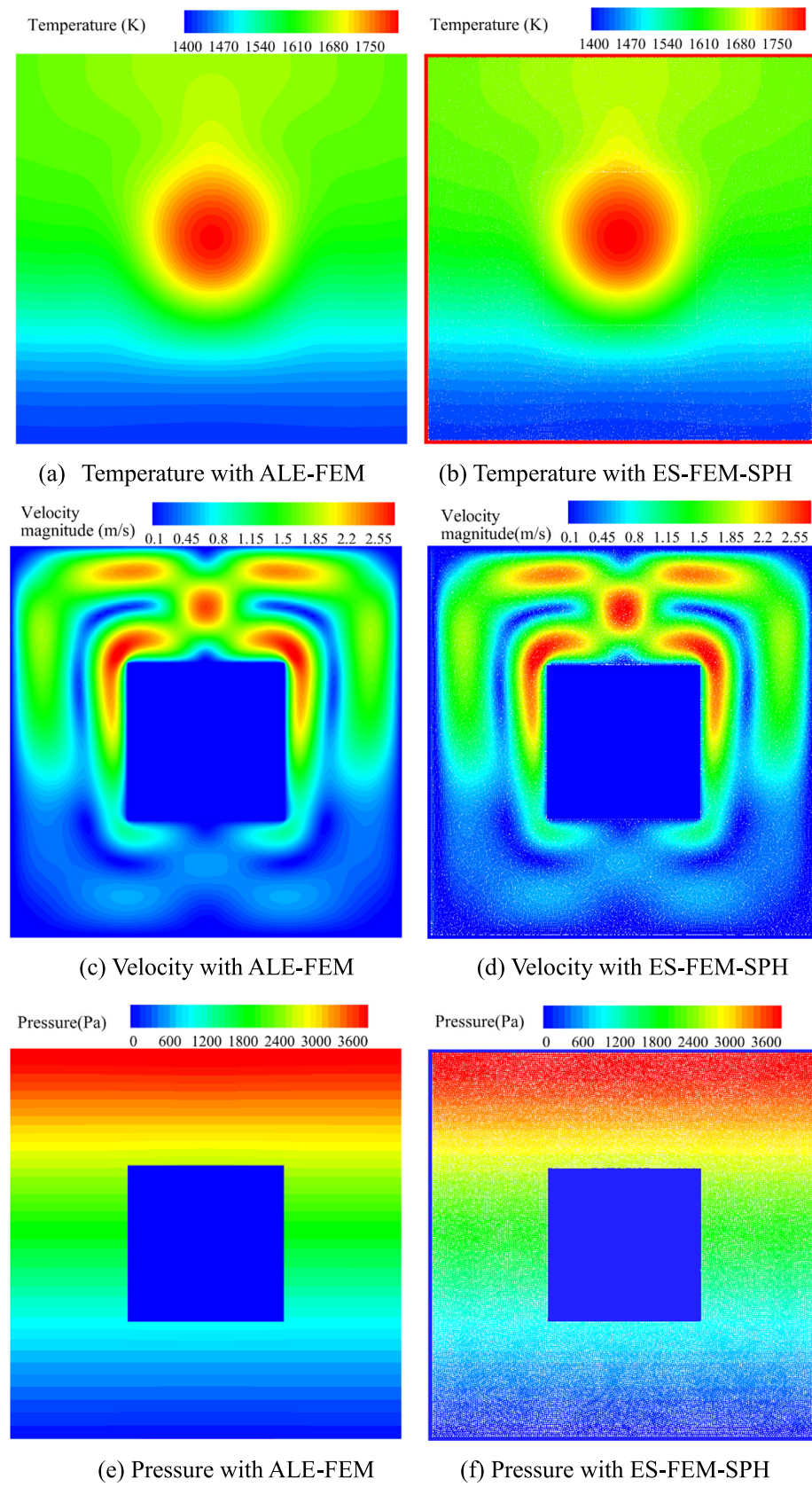


Fig. 16. Thermal energy absorbed by structure and fluid at interface.

and all of the cavity walls. The left vertical wall of square cavity is maintained at a high temperature  $T_H = 1100$ K, while the right vertical wall of square cavity is maintained at a low temperature  $T_C = 100$ K. The up and bottom walls of square cavity are kept adiabatic. At the beginning, the fluid and structure are at rest and isothermal with a temperature  $T_0 = 600$ K. The fluid structure conjugate heat transfer occurs between fluid and flexible beam. Thermal stress and fluid pressure lead to solid deformation, then solid deformation in turn changes the flow field and temperature field. The Saint-Venant-Kirchhoff constitutive model is used for flexible beam. In addition, the material properties of fluid and flexible are given in Table 4. The results of ALE-FEM with re-meshing technique using COMSOL software are used to compare with ES-FEM-SPH coupling approach.

In ES-FEM-SPH model, the flexible beam is discretized by 648 triangular elements and the fluid domain is discretized by 89,280 particles. In ALE-FEM model, the domain is discretized by 102,956 elements. Fig. 19 shows the distributions of velocity, temperature and pressure for



**Fig. 17.** Distribution of temperature, velocity magnitude and pressure at  $t = 10$  s.

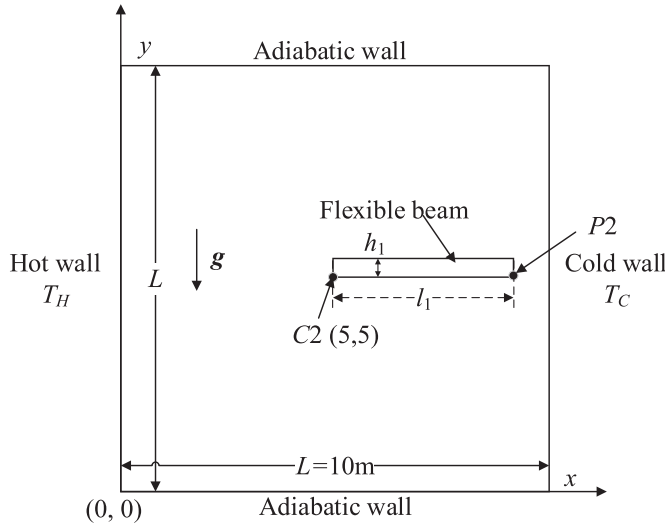


Fig. 18. Convection in a square cavity with a flexible beam.

fluid domain at  $t = 35$  s, respectively. In Fig. 20, the contours of stress and temperature for flexible beam are given out. It can be seen that the results obtained by ES-FEM-SPH coupling approach are in good agreement with those obtained by ALE-FEM. Fig. 21 shows the time history of displacement at point P2, the results of ES-FEM-SPH model agree well with the results of ALE-FEM model. Furthermore, the displacement of point P2 with the adiabatic boundary condition for flexible beam is also given out. It can be seen that the displacement obtained by adiabatic boundary condition is less than the displacement obtained by conjugate heat transfer condition. The high temperature on upper side of elastic beam and low temperature on lower side of flexible beam makes the displacement obtained by conjugate heat transfer larger. Fig. 22 shows the distribution of particles and temperature around flexible beam, the distribution of particle is uniform and the temperature is continuous. All results indicate that the ES-FEM-SPH coupling approach shows good performance for calculating thermal fluid structure interaction problems.

**Table 4**  
Material properties of fluid and flexible beam in Example IV.

Parameters	Value
Fluid density $\rho$	1Kg/m <sup>3</sup>
Solid density $\rho^s$	1000Kg/m <sup>3</sup>
Fluid heat capacity $c$	1J/(KgK)
Solid heat capacity $c^s$	1J/(KgK)
Fluid heat conductivity $k^f$	1W/(mK)
Solid heat conductivity $k^s$	1W/(mK)
Fluid thermal expansion coefficient $\alpha_T^f$	0.071/K
Solid thermal expansion coefficient $\alpha_T^s$	0.0005/K
Acceleration of gravity $g$	10 m/s <sup>2</sup>
Kinematic viscosity $\nu_0$	0.71m <sup>2</sup> /s
Elastic modulus $E$	4.0MPa
Poisson's ratio $\nu$	0.3

## 6. Conclusions

In this paper, for the first time, the ES-FEM-SPH coupling approach is developed for solving the thermal fluid structure interaction problems. In the ES-FEM-SPH coupling approach, the ES-FEM for coupled thermal elastic problems is developed and the SPH method integrated with kernel gradient correction and particle shifting technique is utilized for simulating thermal fluid flows. The ghost particle coupling algorithm is developed for treating fluid structure interaction and fluid structure conjugate heat transfer.

Four typical examples are numerically studied with the present method comparing with results from other sources. From the comparative studies, we conclude that

- 1) The developed ES-FEM based on updated Lagrangian formulation is effective in modeling the coupled thermal elastic problems. The SPH method, after integrating with particle shifting technique and kernel gradient correction, is robust and effective in modeling thermal fluid flows.
- 2) The ghost particle coupling algorithm is developed for treating fluid structure conjugate heat transfer, the continuity of temperature and conservation of energy at interface of fluid and structure are satisfied.
- 3) The developed ES-FEM-SPH model is accurate and effective in modeling thermal fluid structure interaction problems.

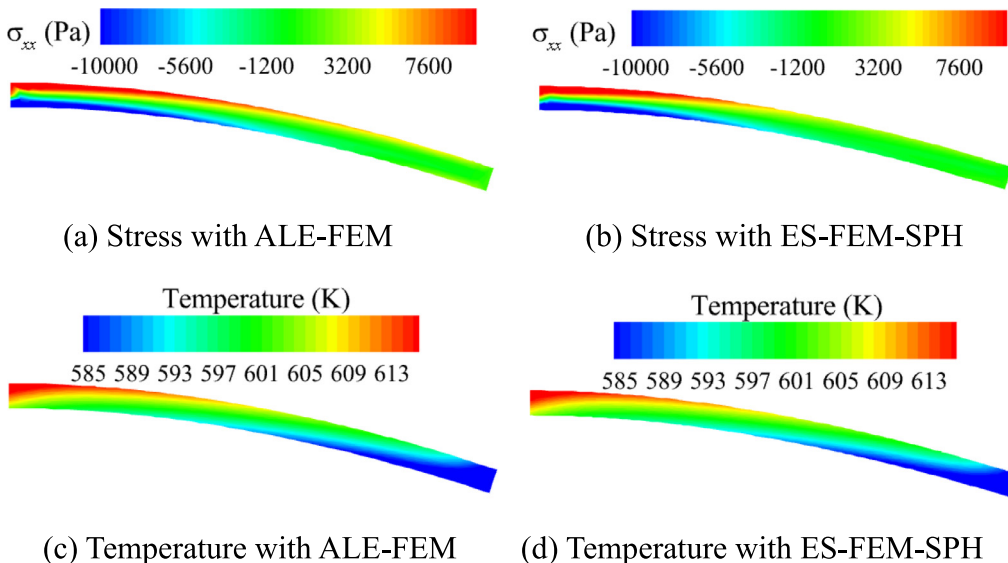
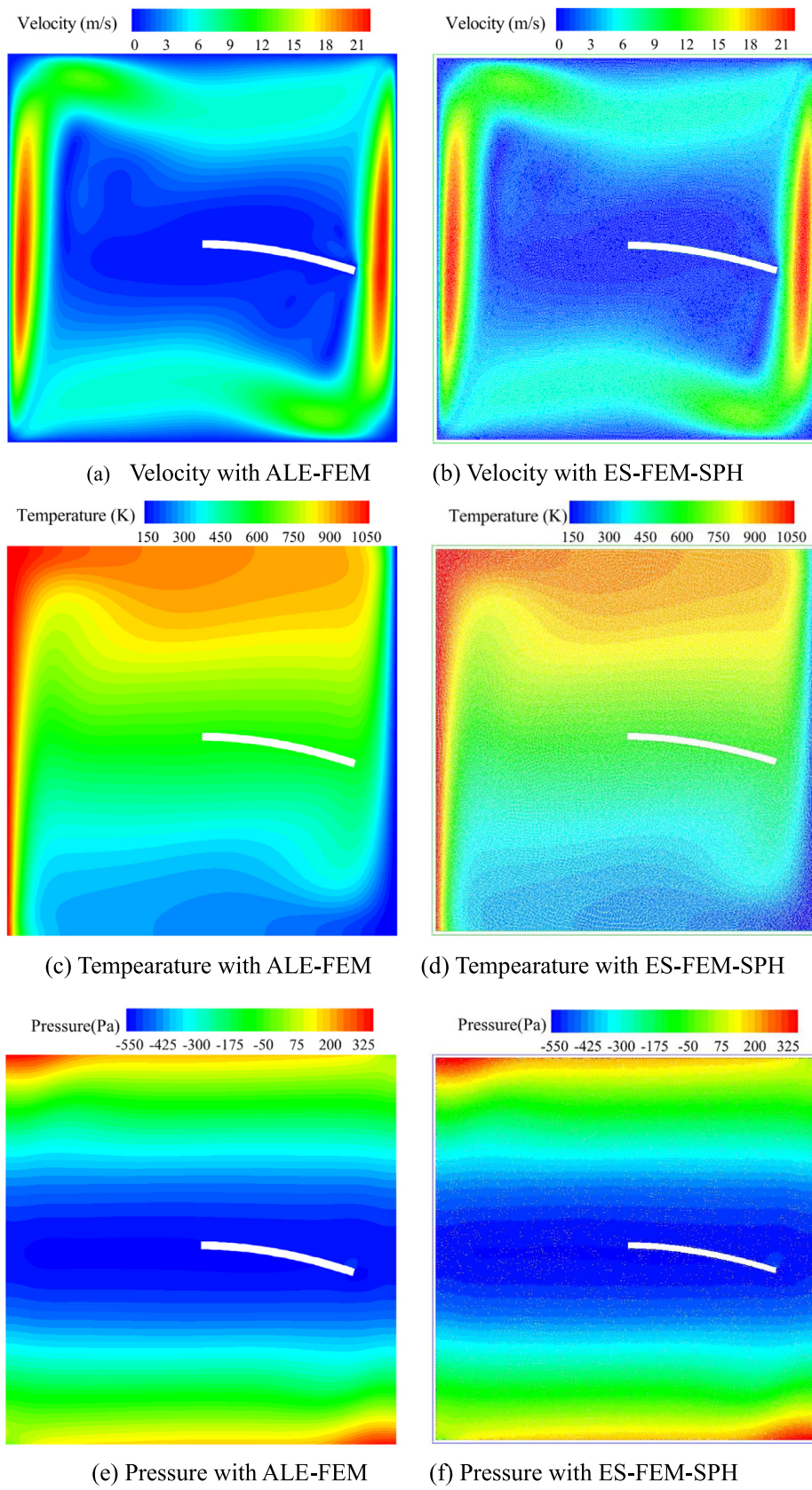


Fig. 20. Distributions of stress and temperature for flexible beam at  $t = 35$  s.



**Fig. 19.** The contours of temperature and the magnitude of velocity at  $t = 35$  s.

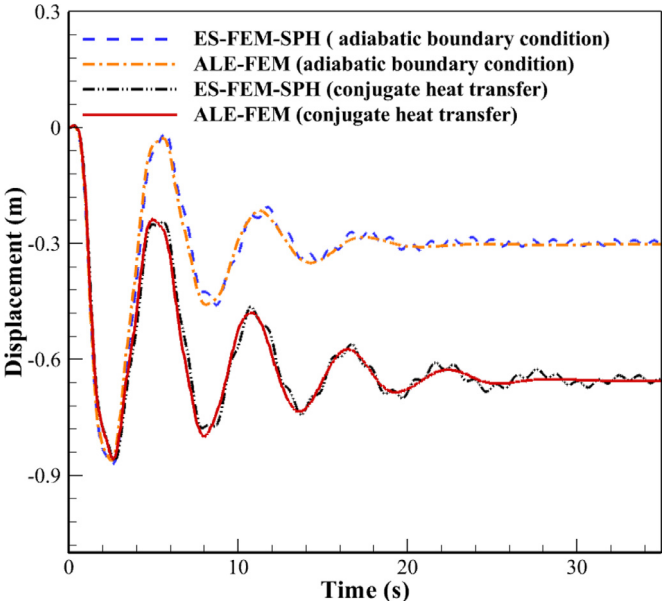


Fig. 21. The time history of displacement of point P2.

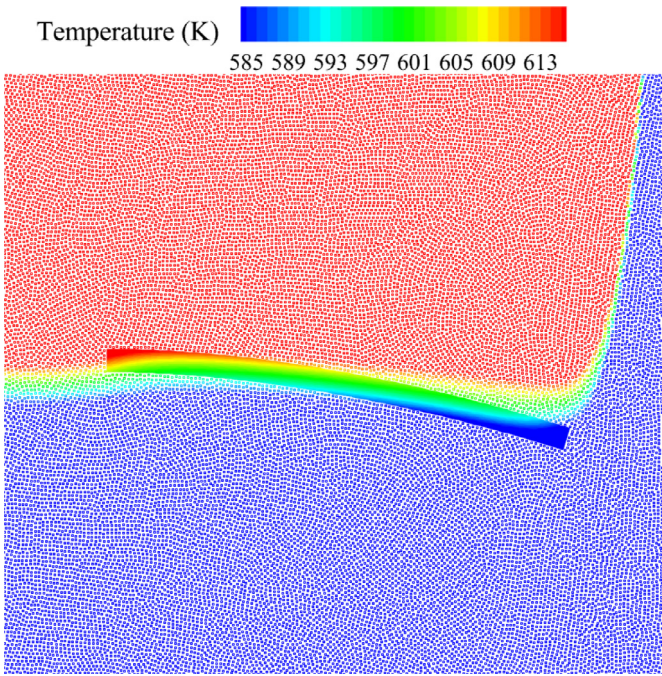


Fig. 22. Distribution of particles and temperature around flexible beam.

#### Declaration of Competing Interest

The authors declare that they have no known competing financial interests or personal relationships that could have appeared to influence the work reported in this paper.

#### CRediT authorship contribution statement

**Ting Long:** Conceptualization, Methodology, Software, Data curation, Writing - original draft. **Pengying Yang:** Investigation, Validation. **Moubin Liu:** Conceptualization, Supervision, Writing - review & editing.

#### Acknowledgments

This work has been supported by the National Natural Science Foundation of China (grant nos. 11902005 and 51779003) and the National Numerical Wind Tunnel Project (grant no NNW2019ZT2-B02).

#### References

- [1] Felicjancik J, Ziolkowski P, Badur J. An advanced thermal-FSI approach of an evaporation of air heat pump. *Trans Inst Fluid-Flow Mach* 2015;129:111–41.
- [2] Al-Amri A, Khanafer K, Bull J, Pop I. Effect of sinusoidal wavy bottom surface on mixed convection heat transfer in a lid-driven cavity. *Int J Heat Mass Transf* 2007;50:1771–80.
- [3] Beeby SP, Tudor MJ, White N. Energy harvesting vibration sources for microsystems applications. *Meas. Sci. Technol.* 2006;17:R175.
- [4] Mills ZG, Aziz B, Alexeev A. Beating synthetic cilia enhance heat transport in microfluidic channels. *Soft Matter* 2012;8:11508–13.
- [5] Yan J, Yan W, Lin S, Wagner GJ. A fully coupled finite element formulation for liquid–solid–gas thermo-fluid flow with melting and solidification. *Comput Methods Appl Mech Eng* 2018;336:444–70.
- [6] Strang G, Fix GJ, Griffin DS. An analysis of the finite-element method. *Math Comput* 1973;41:115–26.
- [7] Reddy JN, Gartling DK. The finite element method in heat transfer and fluid dynamics. CRC Press 2010.
- [8] Thomas JW. Numerical partial differential equations: finite difference methods. Springer Science & Business Media; 2013.
- [9] Eymard R, Gallouët T, Herbin R. Finite volume methods. *Handb Numeri Anal* 2000;7:713–1018.
- [10] Hirt CW, Amsden AA, Cook JL. An arbitrary Lagrangian-Eulerian computing method for all flow speeds. *J Comput Phys* 1974;14:227–53.
- [11] Donea J, Giuliani S, Halleux JP. An arbitrary lagrangian-eulerian finite element method for transient dynamic fluid-structure interactions. *Comput Methods Appl Mech Eng* 1982;33:689–723.
- [12] Peskin CS. The immersed boundary method. *Acta Numerica* 2002;11:479–517.
- [13] Al-Amri A, Khanafer K. Fluid-structure interaction analysis of mixed convection heat transfer in a lid-driven cavity with a flexible bottom wall. *Int J Heat Mass Transf* 2011;54:3826–36.
- [14] Raissi A, Arvin I. A numerical study of the effect of fluid-structure interaction on transient natural convection in an air-filled square cavity. *Int J Therm Sci* 2018;128:1–14.
- [15] Ghalambaz M, Jamesahar E, Ismael MA, Chamkha AJ. Fluid-structure interaction study of natural convection heat transfer over a flexible oscillating fin in a square cavity. *Int J Therm Sci* 2017;111:256–73.
- [16] Ismael MA, Jasim HF. Role of the fluid-structure interaction in mixed convection in a vented cavity. *Int J Mech Sci* 2018;135:190–202.
- [17] Soti AK, Bhardwaj R, Sheridan J. Flow-induced deformation of a flexible thin structure as manifestation of heat transfer enhancement. *Int J Heat Mass Transf* 2015;84:1070–81.
- [18] Z. Cai, B. Thornber, Application of discontinuous galerkin methods for fluid thermal structure interaction problems, (2018).
- [19] Peng D, Merriman B, Osher S, Zhao H, Kang M. A PDE-based fast local level set method. *J Comput Phys* 1999;155:410–38.
- [20] Hirt CW, Nichols BD. Volume of fluid (VOF) method for the dynamics of free boundaries. *J Comput Phys* 1981;39:201–25.
- [21] Koshizuka S, Oka Y. Moving-particle semi-implicit method for fragmentation of incompressible fluid. *Nucl Sci Eng* 1996;123:421–34.
- [22] Koshizuka S, Nobe A, Oka Y. Numerical analysis of breaking waves using the moving particle semi-implicit method. *Int J Numer Methods Fluids* 1998;26:751–69.
- [23] Khayyer A, Tsuruta N, Shimizu Y, Gotoh H. Multi-resolution MPS for incompressible fluid-elastic structure interactions in ocean engineering. *Appl Ocean Res* 2019;82:397–414.
- [24] Gingold RA, Monaghan JJ. Smoothed particle hydrodynamics—theory and application to non-spherical stars. *Mon Not R Astron Soc* 1977;181:375–89.
- [25] Li J, Hamamoto Y, Liu Y, Zhang X. Sloshing impact simulation with material point method and its experimental validations. *Comput Fluids* 2014;103:86–99.
- [26] Zhang F, Zhang X, Sze KY, Lian Y, Liu Y. Incompressible material point method for free surface flow. *J Comput Phys* 2017;330:92–110.
- [27] Sulusky D, Chen Z, Schreyer HL. A particle method for history-dependent materials. *Comput Methods Appl Mech Eng* 1994;118:179–96.
- [28] A. Larese, R. Rossi, E. Oñate, S. Idelsohn, Validation of the particle finite element method (PFEM) for simulation of free surface flows, engineering computations, (2008).
- [29] Gotoh H, Khayyer A. On the state-of-the-art of particle methods for coastal and ocean engineering. *Coast Eng J* 2018;60:79–103.
- [30] Khayyer A, Gotoh H, Falahat H, Shimizu Y. Towards development of enhanced fully-Lagrangian mesh-free computational methods for fluid-structure interaction. *J hydrodyn* 2018;30:49–61.
- [31] Lucy LB. A numerical approach to the testing of the fission hypothesis. *Astron J* 1977;82:1013–24.
- [32] Monaghan JJ, Gingold RA. Shock simulation by the particle method sph. *J Comput Phys* 1983;52:374–89.
- [33] Monteleone A, Marchis MD, Milici B, Napoli E. A multi-domain approach for smoothed particle hydrodynamics simulations of highly complex flows. *Comput Methods Appl Mech Eng* 2018;340.

- [34] Tafuni A, Domínguez J, Vacondio R, Crespo A. A versatile algorithm for the treatment of open boundary conditions in smoothed particle hydrodynamics GPU models. *Comput Methods Appl Mech Eng* 2018;342:604–24.
- [35] A. Khayyer, H. Gotoh, H. Falahaty, Y. Shimizu, An enhanced ISPH-SPH coupled method for simulation of incompressible fluid-elastic structure interactions, computer physics communications, ( 2018 ).
- [36] Zhang Z, Walayat K, Chang J, Liu M. Meshfree modeling of a fluid-particle two-phase flow with an improved SPH method. *Int J Numer Methods Eng* 2018;116:530–69.
- [37] Ji Z, Fu L, Hu XY, Adams NA. A new multi-resolution parallel framework for sph. *Comput Methods Appl Mech Eng* 2019;346:1156–78.
- [38] Wang P-P, Meng Z-F, Zhang A-M, Ming F-R, Sun P-N. Improved particle shifting technology and optimized free-surface detection method for free-surface flows in smoothed particle hydrodynamics. *Comput Methods Appl Mech Eng* 2019;357:112580.
- [39] Ye T, Pan D, Huang C, Liu M. Smoothed particle hydrodynamics (SPH) for complex fluid flows: recent developments in methodology and applications. *Phys Fluid* 2019;31:011301.
- [40] M. Siemann, S. Ritt, Novel particle distributions for SPH bird-strike simulations, computer methods in applied mechanics and engineering, (2018).
- [41] Xiao Y, Dong H. Studying normal and oblique perforation of steel plates with sph simulations. *Int J Appl Mech* 2017;9:1750091.
- [42] Zhang Z, Feng D, Ma T, Liu M. Predicting the damage on a target plate produced by hypervelocity impact using a decoupled finite particle method. *Eng Anal Bound Elem* 2019;98:110–25.
- [43] Szewi K, Pozorski J, Taniere A. Modeling of natural convection with smoothed particle hydrodynamics: non-Boussinesq formulation. *Int J Heat Mass Transf* 2011;54:4807–16.
- [44] Aly AM. Modeling of multi-phase flows and natural convection in a square cavity using an incompressible smoothed particle hydrodynamics. *Int J Numer Methods Heat Fluid Flow* 2015;25:513–33.
- [45] Nguyen MT, Aly AM, Lee S-W. A numerical study on unsteady natural/mixed convection in a cavity with fixed and moving rigid bodies using the ISPH method. *Int J Numer Methods Heat Fluid Flow* 2018;28:684–703.
- [46] Cleary PW, Monaghan JJ. Conduction modelling using smoothed particle hydrodynamics. *J Comput Phys* 1999;148:227–64.
- [47] Trautmann M, Hertel M, Füssel U. Numerical simulation of TIG weld pool dynamics using smoothed particle hydrodynamics. *Int J Heat Mass Transf* 2017;115:842–53.
- [48] Vishwakarma V, Das A, Das P. Steady state conduction through 2D irregular bodies by smoothed particle hydrodynamics. *Int J Heat Mass Transf* 2011;54:314–25.
- [49] Han L, Hu X. SPH modeling of fluid-structure interaction. *J Hydronaut* 2018;30:62–9.
- [50] Liu M, Zhang Z. Smoothed particle hydrodynamics (SPH) for modeling fluid-structure interactions, science china physics. *Mech Astron* 2019;62:984701.
- [51] Sun P, Zhang A-M, Marroone S, Ming F. An accurate and efficient SPH modeling of the water entry of circular cylinders. *Appl Ocean Res* 2018;72:60–75.
- [52] Ng KC, Ng YL, Sheu T, Mukhtar A. Fluid-solid conjugate heat transfer modelling using weakly compressible smoothed particle hydrodynamics. *Int J Mech Sci* 2019;151:772–84.
- [53] Liu M-B, Li S-m. On the modeling of viscous incompressible flows with smoothed particle hydro-dynamics. *J Hydronaut* 2016;28:731–45.
- [54] Vuyst TD, Vignjevic R, Campbell JC. Coupling between meshless and finite element methods. *Int J Impact Eng* 2005;31:1054–64.
- [55] Groenboom PHL, Cartwright BK. Hydrodynamics and fluid-structure interaction by coupled SPH-FE method. *J Hydraul Res* 2009;48:61–73.
- [56] Fourey G, Oger G, Touzé D, Alessandrini B. Violent fluid-structure interaction simulations using a coupled SPH/FEM method. In: Proc. IOP Conference Series: Materials Science and Engineering, IOP Publishing; 2010.
- [57] Yang Q, Jones V, McCue L. Free-surface flow interactions with deformable structures using an SPH-FEM model. *Ocean Eng* 2012;55:136–47.
- [58] Hu D, Long T, Xiao Y, Han X, Gu Y. Fluid-structure interaction analysis by coupled FE-SPH model based on a novel searching algorithm. *Comput Methods Appl Mech Eng* 2014;276:266–86.
- [59] Long T, Hu D, Wan D, Zhuang C, Yang G. An arbitrary boundary with ghost particles incorporated in coupled FEM-SPH model for FSI problems. *J Comput Phys* 2017;350:166–83.
- [60] Zhang Z, Long T, Chang J, Liu M. A smoothed particle element method (SPEM) for modeling fluid-structure interaction problems with large fluid deformations. *Comput Methods Appl Mech Eng* 2019;356:261–93.
- [61] Fourey G, Hermange C, Letouzé D, Oger G. An efficient FSI coupling strategy between smoothed particle hydrodynamics and finite element methods. *Comput Phys Commun* 2017;217.
- [62] Liu GR, Quek SS. The finite element method: a practical course. Butterworth-Heinemann; 2003.
- [63] Liu GR, Dai KY, Nguyen TT. A smoothed finite element method for mechanics problems. *Comput Mech* 2007;39:859–77.
- [64] Chen JS, Wu CT, Yoon S, You Y. A stabilized conforming nodal integration for Galerkin mesh-free methods. *Int J Numer Methods Eng* 2001;50:435–66.
- [65] Liu GR, Nguyen TT, Dai KY, Lam KY. Theoretical aspects of the smoothed finite element method (SFEM). *Int J Numer Methods Eng* 2007;71:902–30.
- [66] Liu GR, Nguyen-Thoi T, Nguyen-Xuan H, Lam KY. A node-based smoothed finite element method (NS-FEM) for upper bound solutions to solid mechanics problems. *Comput Struct* 2009;87:14–26.
- [67] Liu GR, Nguyen-Thoi T, Lam KY. An edge-based smoothed finite element method (ES-FEM) for static, free and forced vibration analyses of solids. *J Sound Vib* 2009;320:1100–30.
- [68] Nguyen-Thoi T, Liu GR, Lam KY, Zhang GY. A face-based smoothed finite element method (FS-FEM) for 3D linear and geometrically non-linear solid mechanics problems using 4-node tetrahedral elements. *Int J Numer Methods Eng* 2009;78:324–53.
- [69] Long T, Hu D, Wan D, Zhuang C, Yang G. An arbitrary boundary with ghost particles incorporated in coupled FEM-SPH model for FSI problems. *J Comput Phys* 2017;350:166–83.
- [70] T. Belytschko, W.K. Liu, B. Moran, K. Elkhodary, Nonlinear finite elements for continua and structures, 2014.
- [71] Zhang ZQ, Liu GR. Solution bound and nearly exact solution to nonlinear solid mechanics problems based on the smoothed FEM concept. *Eng Anal Bound Elem* 2014;42:99–114.
- [72] Rook R, Yildiz M, Dost S. Modeling transient heat transfer using SPH and implicit time integration, numerical heat transfer. Part B: Fundamentals 2007;51:1–23.
- [73] Ng K, Ng Y, Sheu T, Alexiadis A. Assessment of smoothed particle hydrodynamics (SPH) models for predicting wall heat transfer rate at complex boundary. *Eng Anal Bound Elem* 2020;111:195–205.
- [74] Huang C, Zhang D, Shi Y, Si Y, Huang B. Coupled finite particle method with a modified particle shifting technology. *Int J Numer Methods Eng* 2018;113:179–207.
- [75] Liu M-B, Liu G-R. Particle methods for multi-scale and multi-physics. World Scientific; 2016.
- [76] Monaghan JJ, Lattanzio JC, Monaghan JJ, Lattanzio JC. A refined particle method for astrophysical problems. *Astron Astrophys* 1985;149:135–43.
- [77] J.P. Morris, P.J. Fox, Y. Zhu, Modeling Low Reynolds Number Incompressible Flows Using S.P.H., *J Comput Phys*, 136 (1997) 214–26.
- [78] Monaghan JJ. Simulating free surface flows with SPH. *J Comput Phys* 1994;110:399–406.
- [79] Xu R, Stansby P, Laurence D. Accuracy and stability in incompressible sph (ISPH) based on the projection method and a new approach. *J Comput Phys* 2009;228:6703–25.
- [80] Lind SJ, Xu R, Stansby PK, Rogers BD. Incompressible smoothed particle hydrodynamics for free-surface flows: a generalised diffusion-based algorithm for stability and validations for impulsive flows and propagating waves. *J Comput Phys* 2012;231:1499–523.
- [81] Khayyer A, Gotoh H, Shimizu Y. Comparative study on accuracy and conservation properties of two particle regularization schemes and proposal of an optimized particle shifting scheme in ISPH context. *J Comput Phys* 2017;332:236–56.
- [82] Shao JR, Li HQ, Liu GR, Liu MB. An improved SPH method for modeling liquid sloshing dynamics. *Comput Struct* 2012;100-101:18–26.
- [83] Chen J, Dargush GF. Boundary element method for dynamic poroelastic and thermoelastic analyses. *Int J Solids Struct* 1995;32:2257–78.
- [84] Sternberg E. On inertia effects in a transient thermoelastic problem. *J Appl Mech* 1959.
- [85] Wan DC, Patnaik BSV, Wei GW. A new benchmark quality solution for the buoyancy-driven cavity by discrete singular convolution. *Numer Heat Transf Fundam* 2001;40:199–228.